Non-Fermi liquids in the extended Hubbard model

1996 J. Phys.: Condens. Matter 8 9953

(http://iopscience.iop.org/0953-8984/8/48/019)

J. Phys.: Condens. Matter **8** (1996) 9953–9984. Printed in the UK

Non-Fermi liquids in the extended Hubbard model

Qimiao Si

Department of Physics, Rice University, Houston, TX 77251-1892, USA

Received 20 September 1996

Abstract. I summarize recent work on non-Fermi liquids within a certain generalized Anderson impurity model as well as in the large-dimensionality (D) limit of the two-band extended Hubbard model. The competition between local charge and spin fluctuations leads either to a Fermi liquid with renormalized quasiparticle excitations, or to non-Fermi liquids with spin–charge separation. These results provide new insights into the phenomenological similarities and differences between different correlated metals. While presenting these results, I outline a general strategy of local approach to non-Fermi liquids in correlated electron systems.

1. Introduction

Since its introduction four decades ago, Landau's Fermi-liquid theory has been the standard model for interacting many-fermion systems [1]. The theory postulates that at low energies only the quasiparticle excitations play an essential role. The quasiparticles, essentially dressed fermions, can be adiabatically connected to certain non-interacting fermions as we turn off the interaction strength. The Fermi-liquid description has been successful not only for the weakly interacting electrons in simple metals, but also for strongly correlated fermion systems. In this latter category are liquid ^{3}He [2, 3] for which the Fermi-liquid theory was initially formulated, and the metallic states of V_2O_3-based compounds [4, 5], the prototype material displaying the Mott-transition phenomenon [6]. Also included are the 'conventional' heavy fermions [7, 8] such as $CeCu_6$ and UPt_3, in which the masses of the quasiparticles are enhanced by as much as hundreds from the band-theory predictions.

In recent years, a number of strongly correlated materials have emerged which show physical properties anomalous in the context of the canonical Fermi-liquid theory. These include, in addition to the much-studied high-T_c copper oxide superconductors [9], a class of novel heavy fermions [10], d- or f-electron-based metals close to quantum criticality [11, 12], quasi-one-dimensional materials [13, 14], as well as certain artificially fabricated metallic point contacts [15, 16].

The theoretical question, then, is: under what conditions do electron correlations lead to a breakdown of Fermi-liquid theory? In the past few years, several theoretical approaches have been taken to address this question. One approach builds on our understanding of the breakdown of Fermi-liquid theory in one dimension. For weakly interacting one-dimensional fermion systems, the perturbative renormalization group (RG) leads to the g-ology classification of spatially homogeneous metallic states. The possible states are Luttinger liquids or those with divergent CDW, SDW or superconducting correlation functions [17, 18]. In dimensions higher than one, perturbative RG analysis has shown that the Fermi-liquid theory does describe weakly interacting fermion systems with a regular

0953-8984/96/489953+32$19.50

density of states [19–21]. The mechanism for the breakdown of Fermi-liquid theory is necessarily non-perturbative in interaction strength [22].

An alternative approach to non-Fermi liquids uses local physics as a starting point. The motivations behind this approach are multi-fold. First of all, most of the correlated electron systems are transition-metal-, rare-earth- or actinide-based compounds. The dominant electron–electron interactions in these systems are local in space. This is the result of quantum chemistry: the partially filled d or f orbitals are much more contracted than the s and p orbitals of the simple metals and covalent semiconductors, making the intra-site Coulomb interactions by far the largest interaction parameter. Secondly, Anderson- and Kondo-like-impurity models have been studied extensively for more than three decades [23]. In particular, the multi-channel Kondo problem has long been recognized to display RG fixed points of the non-Fermi-liquid variety [24]. Finally, the large-D dynamical mean-field theory [25, 26] opens the door for systematic treatment of the competition between local dynamics and spatial fluctuations.

The work summarized here covers a specific source of local physics towards non-Fermi liquids, namely the competition between local charge (valence) fluctuations and spin fluctuations. This belongs to the domain of mixed-valence physics, a classic problem in condensed-matter theory. It is different from the multi-channel physics for non-Fermi liquids [24, 27]. In the remainder of this section, 1 introduce the problem, define the models, and summarize the essential new results. More detailed discussions of the underlying physics are given in the subsequent sections: sections 2 and 3 focus on the single-impurity generalized Anderson model, and sections 4 and 5 discuss the two-band extended-Hubbard-lattice model.

1.1. Phenomenological considerations

Extensive studies on the heavy-fermion metals have led to a canonical picture for the formation of a Fermi liquid in metals with strong local electron–electron interactions. Figure 1 illustrates the point. Plotted here are the temperature dependence of the Cu-site NMR relaxation rate [28] ($1/T_1$) and that of the electrical resistivity [29] in $CeCu_6$, one of the so-called 'vegetable' heavy fermions. At asymptotically low temperatures, the NMR relaxation rate [30] is linear in temperature, while the electrical resistivity is quadratic in temperature. Both are characteristic of quasiparticle contributions. Simplistically speaking, the number of thermally excited spin excitations is proportional to temperature as a result of the Fermi–Dirac distribution. And each spin excitation contributes a temperature-independent term to the flipping rate of nuclear spins, but a T-linear term to the quasiparticle scattering rate. The latter is again due to the Fermi statistics, which reduces the phase space for quasiparticle–quasiparticle scatterings. The experimental data behave very differently at temperatures above about 5–10 K. Here, the NMR relaxation rate becomes essentially temperature independent, while the temperature dependence of the electrical resistivity is characteristic of Kondo scattering from local moments [23]. A local moment picture serves as a better starting point for describing the f-electron degrees of freedom in this temperature range.

This crossover phenomenon provided the phenomenological basis for the canonical theoretical picture for heavy-fermion metals. In this picture, the f electrons cross over from incoherent moments at high temperatures to being part of the renormalized quasiparticles in a coherent Fermi liquid at the lowest temperatures. This is the lattice analogue of the broad crossover that is known in the solution to the single-impurity Kondo problem [31–33]. In the single-impurity problem, the characteristic crossover temperature is the Kondo energy. In the lattice case, the crossover temperature relates to the coherence energy scale below

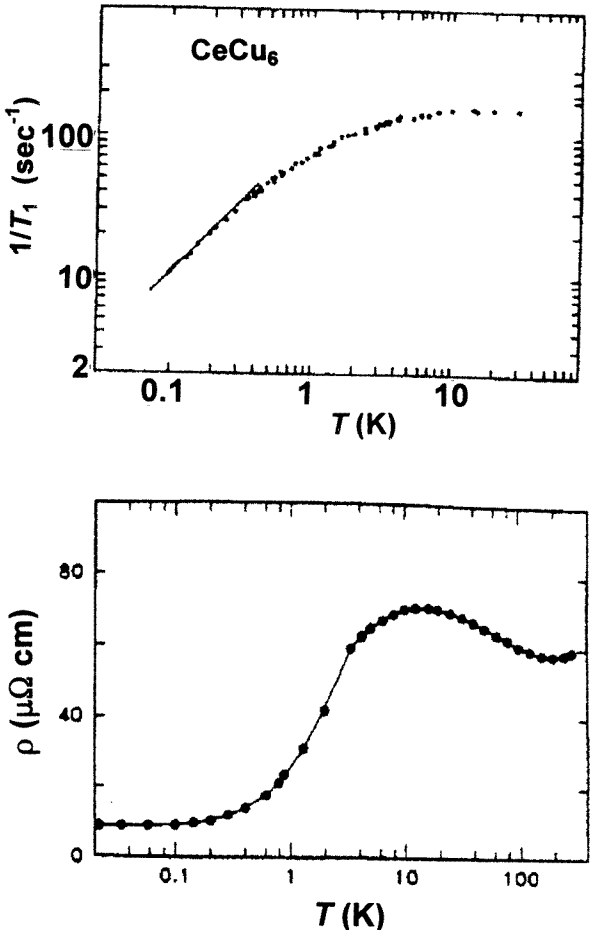

Figure 1. The NMR relaxation rate ($1/T_1$) and electrical resistivity (ρ) as functions of temperature in the heavy-fermion compound $CeCu_6$.

which the elementary excitations are quasiparticles with a heavy mass. The coherence energy acts as the renormalized Fermi energy for the low-energy quasiparticle excitations.

This canonical picture appears to break down for a set of novel f-electron materials [10]. At low temperatures, these materials typically have an electrical resistivity linear in temperature, accompanied by anomalous features in a host of other physical properties. The precise mechanisms for these low-temperature non-Fermi-liquid phenomenologies are at this stage unclear. We refer the readers to the contribution of Miranda *et al* [34] in this Special Issue for a survey of theoretical ideas. The crossover from high to low energies in these systems are only beginning to be addressed [35].

In the normal state of the high-T_c cuprates, the spin dynamics appears to show a crossover qualitatively similar to that of the heavy fermions. Shown in figure 2 are the temperature dependences of the NMR relaxation rate [36] and electrical resistivity [37] in the optimally doped $La_{2-x}Sr_xCuO_4$. The temperature dependence of the NMR relaxation rate behaves in a way reminiscent of that of $CeCu_6$. It has the asymptotic low-temperature T-linear behaviour, crossing over to an essentially temperature-independent

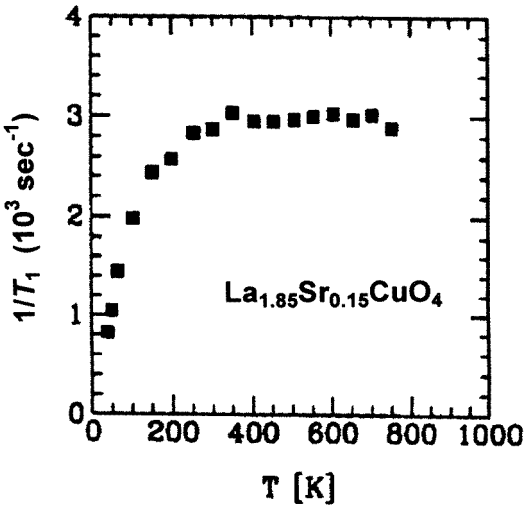

(a)

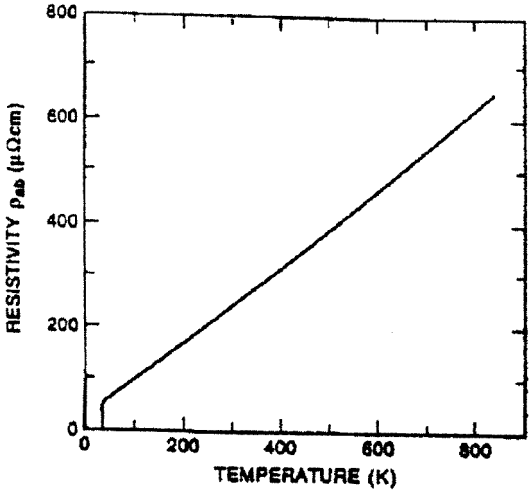

(b)

Figure 2. The NMR relaxation rate ($1/T_1$) and electrical resistivity in the ab-plane (ρ_{ab}) as functions of temperature in the normal state of the high-T_c compound $La_{1.85}Sr_{0.15}CuO_4$.

behaviour at high temperatures. The crossover temperature scale is about 300 K, much higher than that of the heavy fermions. The spin excitations can be thought of as the quasiparticle–quasihole continuum at low temperatures, but as excitations derived from local moments with short-range antiferromagnetic coupling at high temperatures. This picture is corroborated by the neutron scattering results. The low-energy incommensurate peaks are most naturally accounted for in terms of a quasiparticle contribution, while the high-energy broad background is naturally interpreted in terms of short-range local moment correlations [38, 39].

However, when it comes to the temperature dependence of the electrical resistivity, the analogy with the heavy fermions stops. As can be seen in figure 2(b), the electrical

resistivity is linear in temperature over the entire temperature range.

By now, there exists strong evidence that the dominant contribution to the electrical resistivity in the high-T_c cuprates comes from electron–electron scattering [40, 41], as is the case for the heavy fermions. The NMR relaxation rate is of course dominated by the electronic contributions. It is therefore quite unusual that electrons in these systems yield very similar magnetic responses (albeit with different energy scales), but entirely different charge-transport properties. At the microscopic level, both the heavy fermions and copper oxides can be described by a model with a strongly correlated band and a weakly correlated one. The strongly correlated band is formed from the f orbitals in the heavy fermions and from the $3d_{x^2-y^2}$ orbitals in the cuprates. The weakly correlated band is from the non-f orbitals in the heavy fermions and from the oxygen 2p orbitals in the cuprates. For heavy fermions, the point of departure for most theoretical work is the Anderson-lattice model. For cuprates, the model that serves as a sufficiently general microscopic starting point is the three-band extended Hubbard model [42, 43]. Each (planar) unit cell contains one copper 3d orbital and two oxygen 2p orbitals. The non-bonding combination of the 2p orbitals is not expected to play an important role. When this non-bonding combination is ignored, the three-band extended Hubbard model reduces to a two-band Anderson-lattice-like model. We will call this class of models as the two-band extended Hubbard model [44].

Inspired by these considerations, the theoretical question that we ask is: can metallic non-Fermi liquids occur in the two-band extended Hubbard model? We will address this question by incorporating general local interactions allowed by symmetry. Our goal is to treat interactions in a non-perturbative fashion, and seek to classify all of the possible universality classes of this model.

Recent work on this subject can be naturally separated into two categories. Work in the first category concerns exclusively the single-impurity physics. We have generalized the standard Anderson model by including all of the on-site interactions allowed by symmetry [45–48]. The authors of references [49–52, 106] have generalized the standard Anderson model by introducing additional species of screening fermions. Work in the second category deals with the large-D limit of the lattice extended Hubbard model [45–47, 53, 54]. Here we address the physics of the lattice model on the basis of our understanding of the impurity problem.

Connecting the local physics of an impurity model and a lattice model has a long tradition. For instance, the slave-boson large-N approach was first constructed to describe the Fermi-liquid state of the single-impurity Anderson model [55, 56]. The understanding of the impurity problem set the stage for the slave-boson large-N description of the coherent Fermi-liquid state of the Anderson-lattice model [57, 58].

1.2. The generalized Anderson model

The generalized Anderson model that we introduced [45–48] is

$$H = E_d^0 n_d + U n_{d\uparrow} n_{d\downarrow} + \sum_{k\sigma} E_k c_{k\sigma}^\dagger c_{k\sigma} + \sum_{\sigma} t(d_\sigma^\dagger c_\sigma + \text{HC}) + V n_d n_c + J \boldsymbol{S}_d \cdot \boldsymbol{s}_c. \tag{1}$$

Here, $n_{d\sigma} = d_\sigma^\dagger d_\sigma$, $n_d = \sum_\sigma n_{d\sigma}$, $n_c = \sum_\sigma c_\sigma^\dagger c_\sigma$, $\boldsymbol{S}_d = (1/2)\sum_{\sigma,\sigma'} d_\sigma^\dagger \boldsymbol{\tau}_{\sigma\sigma'} d_{\sigma'}$, with τ_x, τ_y, and τ_z being the Pauli matrices, and $\boldsymbol{S}_c = (1/2)\sum_{\sigma,\sigma'} c_\sigma^\dagger \boldsymbol{\tau}_{\sigma\sigma'} c_{\sigma'}$. The first four terms describe the standard Anderson model. For the single-impurity spin-$\frac{1}{2}$ d orbital, the energy level is E_d^0, and the on-site Coulomb repulsion U. For the most part, we will consider only the $U = \infty$ limit. For the spin-$\frac{1}{2}$ conduction c electrons, the energy dispersion is E_k.

$c_\sigma^\dagger = (1/\sqrt{N_{site}}) \sum_k c_{k\sigma}^\dagger$ is the Wannier orbital of the c electrons at the impurity site. It hybridizes with the d electron through the hybridization matrix t.

The last two terms are additional interaction terms allowed by symmetry. V describes a local density–density interaction between the impurity d and local c electrons. In the heavy-fermion literature, this term is called the Falicov–Kimball interaction [59]. J describes the spin-exchange interaction between the d and c electrons. It describes the sum of the direct exchange interaction and the indirect exchange interactions mediated by those high-energy configurations not included in the model Hamiltonian.

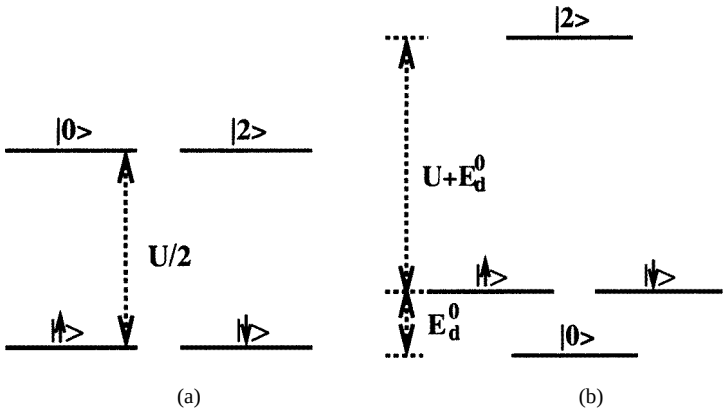

Figure 3. Impurity configurations and energy levels in (a) the symmetric Anderson model and (b) the asymmetric Anderson model.

The standard Anderson model with a featureless conduction electron density of states has already been solved. In the particle–hole- (p–h-) symmetric case, namely for $U + 2E_d^0 = 0$, the impurity d levels are illustrated in figure 3(a). For sufficiently large U, the empty impurity configuration ($|0\rangle$) and the doubly occupied impurity configuration ($|2\rangle \equiv |\uparrow\downarrow\rangle$) can be eliminated through a Schrieffer–Wolff transformation [60]. The result is the Kondo problem with antiferromagnetic exchange interaction. The latter problem is solved by a variety of methods, including the scaling [31], numerical renormalization group (NRG) [32], Bethe *ansatz* [33], and slave-boson large-N methods [56], and conformal field theory [61]. The conclusion is that the low-lying excitations can be well described by the strong-coupling Fermi-liquid fixed point. The local moment is quenched by the conduction electron spin polarization and hence disappears from the low-lying excitation spectrum.

In the p–h-asymmetric case, $U + 2E_d^0 \gg |E_d^0|$, three impurity configurations have to be retained at low energies. This is the mixed-valence problem. It differs from the Kondo problem in that low-lying local charge (valence) fluctuations coexist with spin fluctuations. Historically, a variational study by Varma and Yafet [62], and RG studies of Haldane [63] and Krishnamurthy *et al* [64], the Bethe *ansatz* solution [33] and the slave-boson large-N results [55] have all found that the low-energy behaviour of the mixed-valence problem is described by a strong-coupling, Fermi-liquid fixed point. This fixed point is qualitatively similar to that of the Kondo problem, though quantities such as the Wilson ratio are modified.

In references [45–48], we studied the generalized Anderson impurity model by extending Haldane's RG scheme such that the local charge fluctuations and local spin fluctuations are treated on an equal footing. In the mixed-valence regime, there exist three, and only three, kinds of fixed points. In addition to the aforementioned strong-coupling Fermi-liquid phase, there are two non-Fermi-liquid phases which we termed the weak-coupling phase and the

intermediate phase. The strong-coupling and weak-coupling phases are the direct analogues of the strong-coupling phase of the antiferromagnetic Kondo problem and the weak-coupling phase of the ferromagnetic Kondo problem, respectively. As for the local moment case, the weak-coupling phase of the mixed-valence problem requires that the exchange coupling be ferromagnetic. Therefore, this state is likely be of only academic value for the most part. The possible exception is the double-exchange model for the perovskite manganese oxides [65]. The intermediate phase is unique to the mixed-valence regime. Its existence came as a surprise. In this new phase, spin and charge excitations are separated; the spin susceptibility still has the Fermi-liquid form as in the strong-coupling phase, while the charge susceptibility and the single-particle Green's function have an algebraic behaviour with interaction-dependent exponents. Our RG results are substantiated by the strong-coupling atomic analysis [46] and by the exact solutions at certain exactly soluble points (Toulouse points) [48].

The single-impurity model that Perakis *et al* [49] studied using the NRG is defined as follows:

$$H = E_d^0 n_d + U n_{d\uparrow} n_{d\downarrow} + \sum_{k\sigma} E_k c_{k\sigma}^\dagger c_{k\sigma} + \sum_\sigma t\,(d_\sigma^\dagger c_\sigma + \text{HC}) + V n_d n_c + \sum_{l=1}^{N} V_l n_d n_{cl} + \sum_{l=1}^{N} \sum_{k\sigma} E_k c_{l,k\sigma}^\dagger c_{l,k\sigma} \tag{2}$$

where $c_{l,k\sigma}^\dagger$, for $l = 1, \ldots, N$, describe fermionic bands that interact, but do not hybridize, with the impurity d electron. The screening interactions V_l are introduced so that the Friedel sum rule is satisfied [66].

Reference [49] reported NRG results in the mixed-valence regime (with $U = \infty$). The numerical results for the case of sufficiently large values of the screening interactions V_l were interpreted as displaying divergent charge and spin susceptibilities near the mixed-valence point. Such a phase is not expected from the Coulomb-gas RG analysis. Within the Coulomb-gas RG picture, the effect of screening fermions is to modify the initial conditions of the RG flow [45, 50, 67]. The additional screening channels, while increasing the orthogonality effects, do not participate in the formation of fixed points other than the three mentioned earlier. For sufficiently strong V_l, the Coulomb-gas analysis predicts that the mixed-valence state is the intermediate phase, with divergent charge susceptibility, but *regular* spin susceptibility. While further NRG studies are clearly called for, here we note that the existing numerical data of reference [49] might actually not be inconsistent with our Coulomb-gas RG prediction. The reason is simple. Unlike the charge susceptibility, the spin susceptibility continues to increase when E_d^0 is decreased through the transition regime. A true divergence is therefore hard to detect numerically.

1.3. The extended Hubbard model

The two-band extended Hubbard model is the lattice analogue of the generalized Anderson-model equation (1), and is defined by the following Hamiltonian:

$$H = \sum_i \epsilon_d^0 n_{di} + U \sum_i n_{di\uparrow} n_{di\downarrow} + \sum_{ij,\sigma} t_{ij} c_{i\sigma}^\dagger c_{j\sigma} + \sum_{i\sigma} t\,(d_{i\sigma}^\dagger c_{i\sigma} + \text{HC}) + \sum_i (V n_{di} n_{ci} + J \boldsymbol{S}_{di} \cdot \boldsymbol{s}_{ci}). \tag{3}$$

The notation is essentially the same as in equation (1). The only difference is that we have used ϵ_d^0 to label the d-electron level to emphasize the difference of this quantity in the lattice

model from that of the impurity model E_d^0 (see the discussions around equation (32) below).

The first four terms describe the standard Anderson-lattice model. The spin-$\frac{1}{2}$ d electrons have an infinite on-site Coulomb repulsion U, and an energy level ϵ_d^0. t_{ij} describes the kinetic energy term of the c electrons. At every site, the d and c electrons hybridize with each other through the hybridization matrix t. The last two terms represent the on-site density–density and exchange interactions between the two bands at every site.

Unlike for the single-impurity problem, most of the studies on the Anderson-lattice model in the literature focus on the p–h-asymmetric case. This is because the conventional heavy-fermion metallic states are formed only in the p–h-asymmetric case (the p–h-symmetric case has received renewed interest due to the new developments on the so-called Kondo insulators [68]). We do not know as much about the standard Anderson-lattice model as about the standard single-impurity Anderson model. Only a few of the theoretical methods that have been used in the single-impurity problem are generalizable to the lattice case. This includes the Gutzwiller-like variational wavefunctions [69, 70] and the slave-boson large-N method [57, 58]. All of these approaches have led to the conclusion that the low-energy regime is described by a Fermi liquid with heavy-mass quasiparticles. The slave-boson large-N method has also been applied to the copper oxide model [71]. In the metallic states without long-range order, the solution is again a Fermi liquid.

Our new understandings of the impurity physics, combined with the large-D approach, have led to the conclusion that metallic non-Fermi-liquid solutions are possible in the extended Hubbard model. This conclusion is firmly established in the large-D limit [45–47, 53, 54]. In fact, it turns out that the mixed-valence condition is much easier to realize in the lattice models than in the single-impurity model.

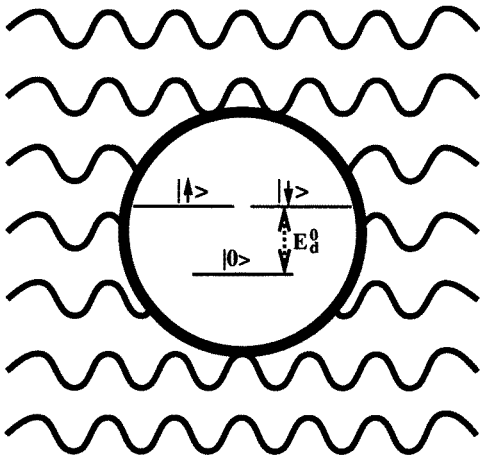

Figure 4. The generalized Anderson model as a three-level system. The wavy lines represent the conduction electron bath.

2. Non-Fermi liquids in the generalized Anderson model: the renormalization group

We focus first on the single-impurity problem. Given that the on-site repulsion is taken to be infinity, the generalized Anderson model can be thought of as a three-level system with a particular form of symmetry breaking. The schematic picture is given in figure 4. The three levels correspond to the three impurity configurations: $|\alpha\rangle = |0\rangle, |\uparrow\rangle, |\downarrow\rangle$. The hybridization

t, density–density interaction V, and spin exchange J couple these three levels to the free-conduction-electron bath. Among the three levels, $|\uparrow\rangle$ and $|\downarrow\rangle$ are degenerate in the absence of an external magnetic field. No symmetry, however, dictates the degeneracy of $|0\rangle$ with $|\uparrow\rangle, |\downarrow\rangle$. It is therefore necessary to keep track of the energy level difference, E_d^0, between $|\uparrow\rangle, |\downarrow\rangle$ and $|0\rangle$. This section summarizes the RG analysis on the three-level system near its criticality. Analysis of certain exactly soluble points—the Toulouse points—is the topic of the next section.

2.1. The Coulomb-gas representation and the renormalization group

The RG analysis is based on a Coulomb-gas representation [31, 63] of the three-level system. This is carried out through an expansion in terms of the hopping amplitudes between the three configurations of the impurity problem. This is an extension of the classic work of Haldane [63] such that the local charge fluctuations and spin fluctuations are treated on an equal footing.

In practice, it is convenient to break the exchange coupling $J\boldsymbol{S}_d \cdot \boldsymbol{s}_c$ into $J_z S_d^z s_c^z + (J_\perp/2)(S_d^+ s_c^- + S_d^- s_c^+)$ where J_z and $J_\perp$ represent the longitudinal and spin-flip components, respectively. V and J_z are diagonal in the impurity configuration basis. Their effects are to cause different scattering potentials for the conduction electrons when they see different impurity configurations. When the impurity configuration is frozen in $|\alpha\rangle$, the scattering potential that the conduction electron of spin σ experiences is V_α^σ:

$$\begin{aligned} V_\sigma^\sigma &= V + J_z/4 \\ V_\sigma^{\bar\sigma} &= V - J_z/4 \\ V_0^\sigma &= 0. \end{aligned} \tag{4}$$

Quite differently, the effects of t and $J_\perp$ terms are to cause quantum transitions between different impurity configurations. Specifically, the hybridization t-term causes transitions between the empty and singly occupied impurity configurations, and the spin-flip $J_\perp$-term causes transitions between the spin-up and spin-down impurity configurations.

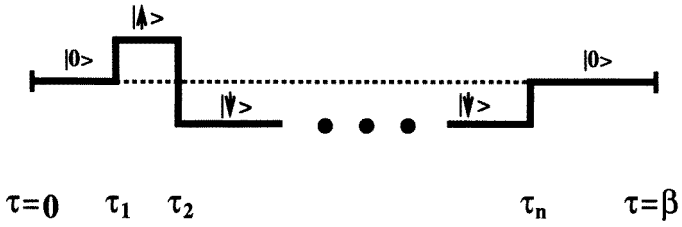

Figure 5. A typical hopping sequence in the atomic representation along the imaginary-time axis $\tau \in [0, \beta \equiv 1/T]$. τ_i, for $i = 1, \ldots, n$, labels the time at which the impurity hops from one configuration to another.

To construct the Coulomb-gas representation, we expand the partition function in terms of t and $J_\perp$, and integrate out the conduction electron degrees of freedom. The resulting form for the partition function is a summation over histories:

$$\frac{Z}{Z_0} = \sum_{\text{history}} \exp(-S[\text{history}]) \tag{5}$$

where Z_0 is the partition function of the free-conduction-electron sea. A history corresponds to a sequence of quantum mechanical hoppings from one impurity state to another along the imaginary-time axis. A transition from impurity state $|\alpha\rangle$ to $|\beta\rangle$ is called a kink (α, β). A history can be specified using the notation $[\alpha_1, \ldots, \alpha_n; \tau_1, \ldots, \tau_n]$ which specifies an (α_i, α_{i+1}) kink at time τ_i. Figure 5 illustrates a particular history. The statistical weight for a given history turned out to be

$$S[\alpha_1, \ldots, \alpha_n; \tau_1, \ldots, \tau_n] = -\sum_i \ln(y_{\alpha_i \alpha_{i+1}}) + \sum_i h_{\alpha_{i+1}} \frac{(\tau_{i+1} - \tau_i)}{\xi_0} + \sum_{i<j} [K(\alpha_i, \alpha_j) + K(\alpha_{i+1}, \alpha_{j+1}) - K(\alpha_i, \alpha_{j+1}) - K(\alpha_{i+1}, \alpha_j)] \ln \frac{(\tau_j - \tau_i)}{\xi_0} \tag{6}$$

where $\xi_0 \sim \rho_0$ is the ultraviolet inverse energy cut-off.

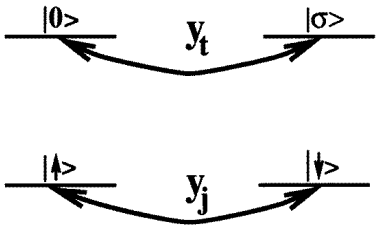

Figure 6. A schematic picture showing that the fugacities of the Coulomb-gas representation correspond to the dimensionless quantum transition amplitudes between the impurity configurations. $y_t = t\xi_0$ is the charge fugacity, and $y_j = J_\perp \xi_0$ the spin fugacity. ξ_0 is the inverse energy cut-off.

This action has the form of a Coulomb gas with two distinctive species of Coulomb 'charges'. The two Coulomb 'charges' correspond to the charge kink and the spin kink, respectively. The fugacities of the two Coulomb 'charges' are

$$\begin{aligned} y_t &\equiv y_{0,\sigma} = t\xi_0 \\ y_j &\equiv y_{\uparrow,\downarrow} = \frac{J_\perp}{2}\xi_0. \end{aligned} \tag{7}$$

As illustrated in figure 6, the charge fugacity y_t corresponds to the hopping amplitude between two local states with different charge quantum numbers. Likewise, the spin fugacity y_j describes the hopping amplitude between the $|\uparrow\rangle$ and $|\downarrow\rangle$ configurations. The fields h_α describe the energy splittings among the three configurations. In the absence of an external magnetic field, $h_0 = -\frac{2}{3}E_d^0\xi_0$ and $h_\sigma = \frac{1}{3}E_d^0\xi_0$.

The logarithmic interactions between the hopping events reflect the reaction of the electron bath towards the changes of the impurity configurations. The interaction strength is characterized by the stiffness constants, $\epsilon_t = -K(0, \sigma)$ and $\epsilon_j = -K(\uparrow, \downarrow)$ which in turn are determined by the bare interaction strength of the original Hamiltonian. Specifically,

$$\begin{aligned} \epsilon_t &= \frac{1}{2}\left[\left(1 - \frac{\delta_\sigma^\sigma - \delta_0^\sigma}{\pi}\right)^2 + \left(\frac{\delta_\sigma^{\bar\sigma} - \delta_0^{\bar\sigma}}{\pi}\right)^2\right] \\ \epsilon_j &= \left(1 - \frac{\delta_\sigma^\sigma - \delta_\sigma^{\bar\sigma}}{\pi}\right)^2 \end{aligned} \tag{8}$$

where $\delta_\alpha^\sigma = \tan^{-1}(\pi\rho_0 V_\alpha^\sigma)$ is the scattering phase shift that the conduction electron bath of spin σ—whose density of states is ρ_0—experiences when the impurity configuration is frozen in $|\alpha\rangle$.

The RG equations describe how the fugacities, stiffness constants, and the symmetry-breaking field flow as we increase the cut-off ξ. We follow the formalism of Cardy [72]. A detailed derivation can be found in references [46]. Here we quote the results:

$$\begin{aligned}
\mathrm{d}y_t/\mathrm{d}\ln\xi &= (1-\epsilon_t)y_t + y_t y_j \\
\mathrm{d}y_j/\mathrm{d}\ln\xi &= (1-\epsilon_j)y_j + y_t^2 \\
\mathrm{d}\epsilon_t/\mathrm{d}\ln\xi &= -6\epsilon_t y_t^2 + \epsilon_j(y_t^2 - y_j^2) \\
\mathrm{d}\epsilon_j/\mathrm{d}\ln\xi &= -2\epsilon_j(y_t^2 + 2y_j^2) \\
\mathrm{d}E_d\xi/\mathrm{d}\ln\xi &= (y_t^2 - y_j^2) + E_d\xi(1-3y_t^2).
\end{aligned} \tag{9}$$

The RG flow of the fugacities determines how the amplitude for making transitions between different impurity configurations are modified as we go towards longer time-scales. When the amplitude grows the system is a Fermi liquid in analogy to the formation of Fermi liquid in the usual Kondo problem. When this amplitude renormalizes to zero, quantum coherence is destroyed and Fermi-liquid theory breaks down. This way, we cast the breakdown of Fermi-liquid theory in the framework of the macroscopic-quantum-coherence (MQC) problem [73]. The transitions between Fermi-liquid and non-Fermi-liquid phases are extensions of the well known localization transitions in the MQC problem with one essential difference. Here we deal with a special *three-level* system instead of the canonical *two-level* system studied in the MQC literature. This leads to a richer phase diagram that we describe below.

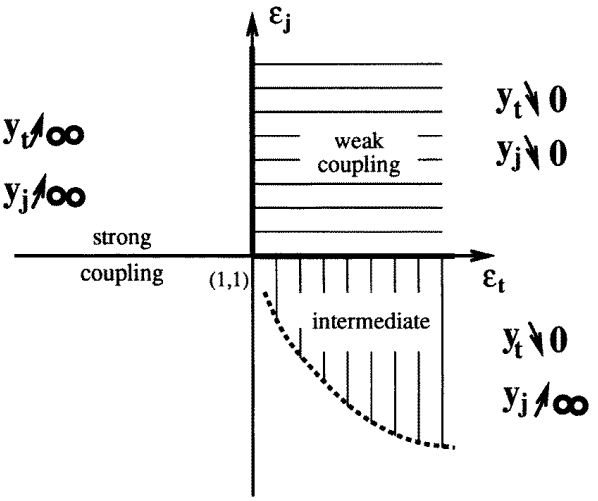

Figure 7. The phase diagram of the generalized Anderson-model equation (1) in the mixed-valence regime. Here ϵ_t and ϵ_j label the charge- and spin-stiffness constants defined in the text. The vertical thick line, the horizontal thick line, and the dashed line are the boundaries between the different mixed-valence states. The dashed line is schematic.

2.2. Universality classes

Solving the RG flow establishes the existence of three, and only three, mixed-valence fixed points. The phase diagram for the mixed-valence regime is specified in terms of the stiffness constants ϵ_t and ϵ_j and is given in figure 7.

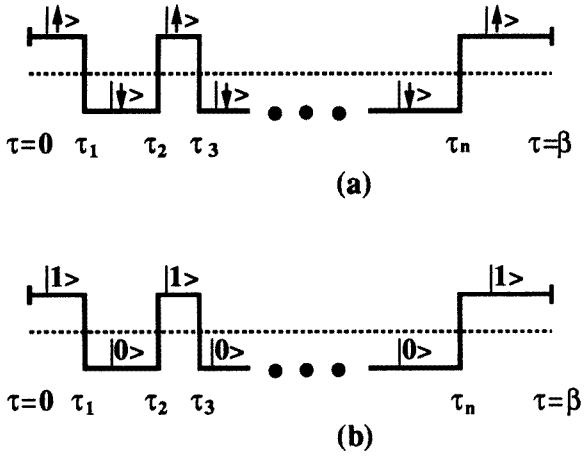

Figure 8. Hopping sequences in the atomic representation for (a) the usual spin Kondo problem and (b) the charge Kondo problem, i.e., the resonant-level model.

The physical meaning of the strong-coupling, weak-coupling, and intermediate phases is most transparent when the three-level system is thought of as the hybrid of a two-level spin Kondo problem and a two-level charge Kondo problem. In the spin Kondo problem, the 'charge' of the corresponding Coulomb gas corresponds to the spin kink. A history of n spin kinks is shown in figure 8(a). The parameters of the Coulomb gas are the spin fugacity $y_j = J_\perp \xi_0$ and the spin-stiffness constant $\epsilon_j' = [1 - (2/\pi)\tan^{-1}(\pi \xi_0 J_z/4)]^2$. The RG flow is well known [31] and is given in figure 9(a). For antiferromagnetic J_z, i.e. $\epsilon_j < 1$, the flow is towards the strong-coupling, Fermi-liquid fixed point. While for ferromagnetic J_z, i.e. $\epsilon_j > 1$, the flow is towards a line of weak-coupling fixed points. In a weak-coupling fixed point, there is an asymptotically decoupled spin.

The charge Kondo effect describes the physics of the so-called resonant-level model in the presence of a p–h symmetry. The spinless version of the Hamiltonian (1) with $E_d^0 = 0$ reduces to the resonant-level model. It was realized some time ago [74, 75] that the resonant-level model can be asymptotically mapped onto the anisotropic Kondo problem, with the hybridization t and the density–density interaction V playing the roles of $J_\perp$ and J_z, respectively. The 'charge' of the corresponding Coulomb gas describes a charge kink. A history of charge kinks is illustrated in figure 8(b). The charge fugacity is $y_t = t\xi_0$ and the charge-stiffness constant is $\epsilon_t' = (1/2)[1 - (2/\pi)\tan^{-1}(\pi \xi_0 V/2)]^2$. The RG flow is given in figure 9(b). The flow is towards a strong-coupling Fermi-liquid fixed point for $\epsilon_t' < 1$, but towards a line of weak-coupling fixed points for $\epsilon_t' > 1$. In a weak-coupling fixed point, the charge degree of freedom is asymptotically decoupled. Note that $\epsilon_t' > 1$ corresponds to $-V > -V^{crit} = (2/\pi\rho_0)\tan[(\sqrt{2}-1)\pi/2]$, i.e., a range of finite attractive density–density interaction. It is the charge analogue of the ferromagnetic interaction.

With this background on the charge sector alone and the spin sector alone, the meaning of the strong-coupling phase of the mixed-valence problem is transparent. Both the spin

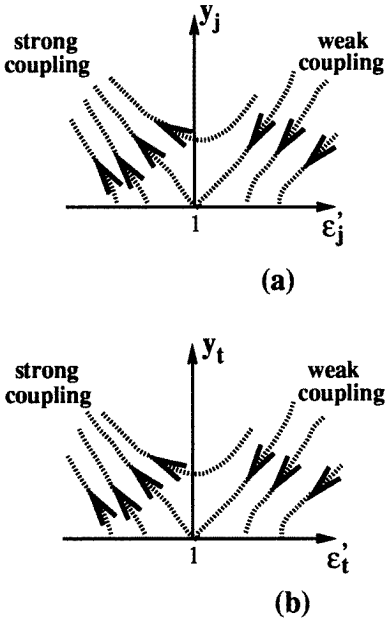

Figure 9. The RG flows for (a) the usual spin Kondo problem and (b) the resonant-level model.

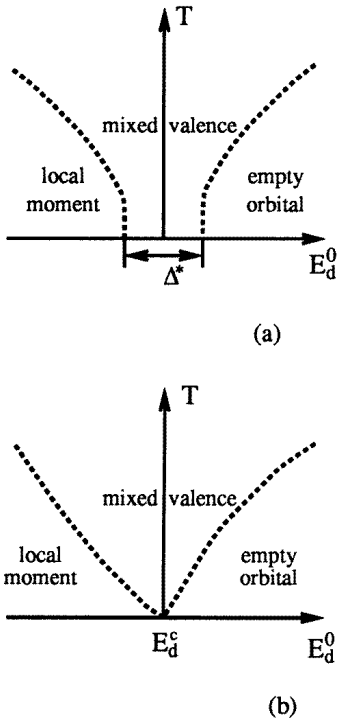

Figure 10. Crossover diagrams in terms of temperature (T) and the impurity level (E_d^0) (a) for the strong-coupling phase where Δ^* is the renormalized resonance width; and (b) for the intermediate phase where E_d^c labels the critical impurity level.

and charge Kondo problems are in the strong-coupling regime; rapid fluctuations between all three local configurations take place and the conduction electrons quench both the charge and spin degrees of freedom of the impurity. It is expected that this phase is a Fermi liquid. A large-N analysis of this regime indeed gives rise to this [46]. So do the exact solutions of the two strong-coupling Toulouse points (see the next section). Likewise, in the weak-coupling phase, neither the local charge nor the local spin degrees of freedom is quenched. Both the spin and charge Kondo problems are in the weak-coupling regime, and all three atomic configurations decouple asymptotically at low energies. The weak-coupling phase requires that the spin-exchange interaction be ferromagnetic. It is therefore very likely to be of only academic value with the possible exception of the double-exchange model.

The unexpected phase is the intermediate phase. Here, the local spin degrees of freedom are quenched, but the local charge degrees of freedom are not. The charge Kondo problem is in the weak-coupling regime despite the fact that the spin Kondo problem is in the strong-coupling regime. There are *two* local configurations carrying different charges which are decoupled asymptotically. The RG analysis establishes this as an allowed phase. The alternative situation, with the spin Kondo problem being in the weak-coupling situation and at the same time the charge Kondo problem being in the strong-coupling case, is not allowed: a relevant charge flipping (hybridization) drives the spin flipping relevant. The domain of attraction of the intermediate phase spans the parameter range within $\epsilon_t > 1$ and

$\epsilon_j < 1$. The RG analysis cannot specify the precise boundary between the strong-coupling and intermediate phases; the dashed line is only schematic. In terms of the parameters of the Hamiltonian (1), in which the density–density interaction V is on site, this domain corresponds to a region with antiferromagnetic exchange interaction J and attractive V. Taking V as an effective parameter this condition can be satisfied in a variety of realistic models with all interactions repulsive [47]. Finite-range interactions also help to realize these phases, as discussed in the context of impurity models [49, 50] and in lattice models [54] (see section 5). The transition between the different regimes is analogous to the localization phase transition studied in the context of the macroscopic-quantum-coherence problem [73] and more recently in the context of transport through constrictions in interacting quantum wires [76].

There is one important difference in symmetry between the asymmetric Anderson model and the p–h-symmetric resonant-level model. The p–h-symmetric resonant-level model has a U(1) symmetry which ensures that the impurity level stays at the Fermi energy of the conduction electron sea. Equivalently, the singly occupied configuration and the empty configuration are guaranteed to be degenerate by symmetry. This degeneracy is responsible for the charge Kondo effect. In the case of the asymmetric Anderson model, no symmetry protects the degeneracy of the singly occupied and the empty impurity configurations. Degeneracy can be achieved only through fine tuning the bare impurity level. The condition for this degeneracy is none other than the condition for mixed valency.

The phase diagram given in figure 7 applies only to the mixed-valence regime. When the mixed-valence condition is not satisfied, the impurity level is either too far below the Fermi energy or too far above the Fermi energy. They correspond to the local moment and empty orbital regimes, respectively. How far is too far away from the Fermi energy depends on whether the corresponding mixed-valence state falls in the strong-coupling, weak-coupling, or intermediate domain. This crossover from local moment, mixed valence, to the empty orbital regimes is specified in the temperature versus impurity level space in figure 10.

Figure 10(a) specifies the finite-temperature crossover for the strong-coupling case. At zero temperature, the mixed-valence crossover extends over a scale of $\sim\Delta^*$, the renormalized resonance width. The value of Δ^* depends, of course, on where we are in the phase diagram of figure 7. It is finite within the strong-coupling domain. As we approach the phase boundary to the intermediate or weak-coupling phases, Δ^* vanishes in a Kosterlitz–Thouless fashion:

$$\Delta^* \approx (\rho_0)^{-1} \exp[-1/\sqrt{\epsilon^{crit} - \epsilon}] \tag{10}$$

where $\epsilon^{crit} - \epsilon$ measures the distance from the phase boundary.

For the intermediate phase, $\Delta^* = 0$, and the mixed-valence point is a zero-temperature critical point. At finite temperatures, there are three energy parameters: temperature (T), the running symmetry-breaking field $\delta E_d(T) \sim (E_d^0 - E_d^c) - \Delta_0(T\xi_0)^{(2\epsilon_i^*-1)}$, and the running resonance width $\Delta(T) \sim \Delta_0(T\xi_0)^{(2\epsilon_i^*-1)}$ (where $\Delta_0 \approx \pi\rho_0 t^2$ is the bare resonance width). The critical behaviour associated with the mixed-valence critical point occurs when $|\delta E_d(T)| < \Delta(T) < T$. This condition specifies the following crossover scale:

$$T' \sim \frac{1}{\xi_0} |(E_d^0 - E_d^c)/\Delta_0|^{1/(2\epsilon_i^*-1)}. \tag{11}$$

The correlation functions assume the form characteristic of the intermediate phase at $T > T'$ for a given E_d^0, or equivalently, for a given temperature, when E_d^0 is tuned to the range

$$|E_d^0 - E_d^c| < \Delta_0(T\xi_0)^{(2\epsilon_i^*-1)}. \tag{12}$$

The intermediate mixed-valence regime is a manifestation of the quantum critical phenomenon in the context of quantum impurity models [77].

2.3. Further remarks

Our most interesting finding in the mixed-valence regime is the existence of a new phase, the intermediate phase. The Coulomb-gas RG analysis provides the qualitative physical picture of the intermediate phase: spin excitations are quasiparticle-like, and charge excitations incoherent. However, the Coulomb-gas RG analysis is not capable of determining the precise forms of the correlation functions for the intermediate phase (neither is it for the strong-coupling phase, for that matter). This calls for alternative means through which correlation functions can be calculated explicitly. In the next section, we present explicit results for the correlation functions near several exactly soluble points.

The Coulomb-gas representation is based on the dilute-instanton expansion. The RG analysis, while non-perturbative in the stiffness constants, is perturbative in terms of the fugacities. It is in principle possible that additional fixed points, not captured by the dilute-instanton expansion, may occur. An example for the latter arises in the related, though qualitatively different, problem of tunnelling through a point contact in a Luttinger liquid [76, 78]. One way to probe the nature of the fixed points is to carry out a strong-coupling atomic analysis, in the same spirit that Nozières did for the usual Kondo problem [79]. Namely, one analyses whether the couplings are stable around the point where the couplings associated with the relevant fugacities take infinite values. We found that these points are indeed stable [46], giving some support to the assertion that the Coulomb-gas RG classification of the universality classes is complete. This analysis of course does not completely rule out the existence of more fixed points. This issue became even more urgent due to the bosonization work of references [52, 51] which reported fixed points not expected from the Coulomb-gas RG picture. It turned out that, as discussed in some detail in the next section, there are some technical subtleties with the application of the bosonization method to the mixed-valence problem. When these subtleties are taken care of, the bosonization results became consistent with the Coulomb-gas RG predictions.

3. Non-Fermi liquids in the generalized Anderson model: Toulouse points

There are three particular combinations of the interactions [48] where the model is exactly soluble [80]. These points in the interaction parameter space are the mixed-valence counterparts of the usual Toulouse point of the Kondo problem [81, 31], and are naturally called the Toulouse points of the mixed-valence problem.

We identify the possible Toulouse points using the bosonization method [42]. Given that the interaction occurs at $\boldsymbol{r} = 0$ only, we need to keep only the s-wave component of the conduction electrons. This s-wave component is defined on the radial axis, $r \in [0, +\infty)$, and can be further decomposed into outgoing and incoming components. In a standard fashion, we extend to the full axis, $x \in (-\infty, +\infty)$, by retaining only one chiral component, which we denote by $\psi_\sigma(x)$. We can then introduce a boson representation for the $\psi_\sigma(x)$-field. At the origin,

$$\psi_\sigma^\dagger(x=0) = F_\sigma^\dagger \frac{1}{\sqrt{2\pi a}} \mathrm{e}^{\mathrm{i}\Phi_\sigma}. \tag{13}$$

Here, a is a cut-off scale which can be taken as a lattice spacing. Φ_σ is the shorthand

notation for $\Phi_\sigma(x=0)$:

$$\Phi_\sigma = \sum_{q>0} \sqrt{\frac{2\pi}{qL}} (-\mathrm{i} b^\dagger_{q\sigma} \mathrm{e}^{-qa/2} + \mathrm{i} b_{q\sigma} \mathrm{e}^{-qa/2}) \tag{14}$$

where $b_{q\sigma}$ and $b^\dagger_{q\sigma}$ are the Tomonaga bosons, and L is the length of the dimension and is taken to be infinite in the end. An important point is that Φ_σ depends only on the $q \neq 0$ components of the Tomonaga bosons. In equation (13), the operator $F^\dagger_\sigma$, and its adjoint F_σ, are the so-called Klein factors. They have to be introduced in order to preserve the anti-commutation relation between fermions of different spin components. They should be thought of as acting on the $q = 0$ sector of the Hilbert space for the Tomonaga bosons. More precisely, the Klein factors can be defined as the raising and lowering operators, respectively, in such a Hilbert space [18, 82, 83]. These operators are unitary, and anticommute among the different spin species. Furthermore, they commute with $b_{q\sigma}$ and $b^\dagger_{q\sigma}$ for $q \neq 0$ and, hence, also with Φ_σ.

The generalized Anderson model can be rewritten in the bosonized form:

$$\begin{aligned}
H &= H_0 + E^0_d \sum_\sigma X_{\sigma\sigma} + H_{\perp t} + H_{\perp j} + H_V \\
H_0 &= \frac{v_F}{4\pi} \int \mathrm{d}x \left[\left(\frac{\mathrm{d}\Phi_s}{\mathrm{d}x} \right)^2 + \left(\frac{\mathrm{d}\Phi_c}{\mathrm{d}x} \right)^2 \right] \\
H_{\perp t} &= \frac{t}{\sqrt{2\pi a}} \sum_\sigma [X_{\sigma 0} F_\sigma \mathrm{e}^{-\mathrm{i}(1/\sqrt{2})\Phi_c} \mathrm{e}^{-\mathrm{i}\sigma(1/\sqrt{2})\Phi_s} + \mathrm{HC}] \\
H_{\perp j} &= \frac{J_\perp}{4\pi a} [X_{\uparrow\downarrow} F^\dagger_\downarrow F_\uparrow \mathrm{e}^{-\mathrm{i}\sqrt{2}\Phi_s} + \mathrm{HC}] \\
H_V &= \sum_\alpha X_{\alpha\alpha} \left[\left(\frac{\delta^s_\alpha}{\pi\rho_0} \right) \left(\frac{1}{2\pi} \right) \left(\frac{\mathrm{d}\Phi_s}{\mathrm{d}x} \right)_{x=0} + \left(\frac{\delta^c_\alpha}{\pi\rho_0} \right) \left(\frac{1}{2\pi} \right) \left(\frac{\mathrm{d}\Phi_c}{\mathrm{d}x} \right)_{x=0} \right]
\end{aligned} \tag{15}$$

where we have used $n_d = \sum_\sigma X_{\sigma\sigma}$, $d^\dagger_\sigma = X_{\sigma 0}$, $S^+_d = X_{\uparrow\downarrow}$, and $S^z_d = (X_{\uparrow\uparrow} - X_{\downarrow\downarrow})/2$. $X_{\alpha\beta} = |\alpha\rangle\langle\beta|$ are the Hubbard operators. The requirement that α, β take three, and only three, impurity configurations, $|0\rangle$ and $|\sigma\rangle = d^\dagger_\sigma|0\rangle$, amounts to the following constraint:

$$X_{\uparrow\uparrow} + X_{\downarrow\downarrow} + X_{00} = 1. \tag{16}$$

In equation (15), $\Phi_{c,s} \equiv (\Phi_\uparrow \pm \Phi_\downarrow)/\sqrt{2}$ are the charge and spin bosons, respectively. $\delta^c_\alpha \equiv (1/\sqrt{2}) \sum_\sigma \delta^\sigma_\alpha$ and $\delta^s_\alpha \equiv (1/\sqrt{2}) \sum_\sigma \sigma \delta^\sigma_\alpha$. $v_F = 1/2\pi\rho_0$ is the Fermi velocity.

The Toulouse points are derived through applying a canonical transformation to the Hamiltonian equation (15) and demanding that the transformed $H_{\perp t}$ and $H_{\perp j}$ have simple forms and, simultaneously, the transformed H_V vanishes. Three such Toulouse points exist. The details are given in reference [48]. In the following, we only quote the effective Hamiltonian, and the results for the single-particle, spin–spin, and charge–charge correlation functions, at each of these Toulouse points.

3.1. Strong-coupling Toulouse point I

The first Toulouse point corresponds to $\epsilon_t = 0$ and $\epsilon_j = 0$. According to the phase diagram (figure 7) of the Coulomb-gas RG analysis, this point lies deep in the strong-coupling, Fermi-liquid region.

To write down the effective Hamiltonian, we need to introduce pseudoboson operators $b_\sigma^\dagger$ and $b_0^\dagger$ defined as follows:

$$\begin{aligned} X_{\sigma\sigma'} &= f_\sigma^\dagger f_{\sigma'} \\ X_{\sigma 0} &= f_\sigma^\dagger b_0 \\ X_{00} &= b_0^\dagger b_0 \\ b_\sigma^\dagger &= f_\sigma^\dagger F_{\bar\sigma}^\dagger. \end{aligned} \tag{17}$$

Note that the pseudoboson operator $b_\sigma^\dagger$ incorporates a Klein operator associated with the conduction electron degrees of freedom. In terms of these operators, the constraint equation (16) can be rewritten as $\sum_\sigma b_\sigma^\dagger b_\sigma + b_0^\dagger b_0 = 1$. The effective Hamiltonian can then be conveniently written as

$$\begin{aligned} H_{eff}^A &= H_0 + H_{3l} + \Delta H \\ H_{3l} &= E_d^0\left(\sum_\sigma b_\sigma^\dagger b_\sigma - b_0^\dagger b_0\right) + \frac{t}{\sqrt{2\pi a}}\sum_\sigma (b_\sigma^\dagger b_0 + \text{HC}) - \frac{J_\perp}{4\pi a}(b_\uparrow^\dagger b_\downarrow + \text{HC}) \\ \Delta H &= \left(\frac{\kappa_c}{2\pi\rho_0}\right)\left(\sum_\sigma b_\sigma^\dagger b_\sigma - b_0^\dagger b_0\right)\left(\frac{1}{2\pi}\right)\left(\frac{\mathrm{d}\Phi_c}{\mathrm{d}x}\right)_{x=0} \\ &\quad + \left(\frac{\kappa_s}{2\pi\rho_0}\right)\left(\sum_\sigma \sigma b_\sigma^\dagger b_\sigma\right)\left(\frac{1}{2\pi}\right)\left(\frac{\mathrm{d}\Phi_s}{\mathrm{d}x}\right)_{x=0} \end{aligned} \tag{18}$$

where κ_c and κ_s measure the deviation from the Toulouse point. This effective Hamiltonian is composed of three parts. H_{3l} is the Hamiltonian for the three isolated levels, $b_\uparrow^\dagger|\text{vac}\rangle$, $b_\downarrow^\dagger|\text{vac}\rangle$, and $b_0^\dagger|\text{vac}\rangle$, where $|\text{vac}\rangle$ denotes the vacuum state. The t and $J_\perp$ are transverse fields, and E_d^0 provides a longitudinal field. H_0 describes the free-spin and free-charge bosonic fields. Finally, ΔH is the dissipative term coupling the three levels to the bosonic baths. The effective Hamiltonian therefore is a three-level generalization of the two-level 'spin'-boson problem [84, 73].

All of the correlation functions of this three-level 'spin'-boson problem can be calculated explicitly. The results for the single-particle Green's function $G_d(\tau) = -\langle T_\tau d_\sigma(\tau) d_\sigma^\dagger(0)\rangle$, the density–density correlation function $\chi_\rho(\tau) = \langle T_\tau n_d(\tau) n_d(0)\rangle$, the longitudinal and transverse spin–spin correlation functions $\chi_\sigma^{zz}(\tau) = \langle T_\tau S^z(\tau) S^z(0)\rangle$ and $\chi_\sigma^{+-}(\tau) = \langle T_\tau S^-(\tau) S^+(0)\rangle$ are given as follows:

$$\begin{aligned} G_d(\tau) &\sim \frac{\rho_0}{\tau} \\ \chi_\sigma^{-+}(\tau) &\sim \left(\frac{\rho_0}{\tau}\right)^2 \\ \chi_\sigma^{zz}(\tau) &\sim \left(\frac{\kappa_s}{2\pi\rho_0 h_s}\right)^2\left(\frac{\rho_0}{\tau}\right)^2 \\ \chi_\rho(\tau) &\sim \left(\frac{\kappa_c}{2\pi\rho_0 h_c}\right)^2\left(\frac{\rho_0}{\tau}\right)^2 \end{aligned} \tag{19}$$

where $h_s = J_\perp/4\pi a$ and $h_c = t/\sqrt{2\pi a}$. A long-time $1/\tau$ behaviour for the single-particle Green's function, together with the $1/\tau^2$ behaviour for the two-particle correlation functions, imply that the system is a Fermi liquid. Therefore, this Toulouse point describes the strong-coupling phase.

Unlike for the Kondo problem, keeping track of the anticommutation relation between fermions of different spins in the boson representation plays an essential role. Had we not included the Klein operator in the boson representation of the fermion operator equation (13), the pseudoboson operator b_σ defined in equation (17) would not have included the additional Klein operator (it would then be a pseudofermion, as a matter of fact). The sign of the $J_\perp$-term would be reversed. It can be seen by diagonalizing the three-level atomic problem, H_{3l}, that a level crossing would arise as E_d^0 is varied. The critical value of E_d^0 where levels cross would correspond to a non-Fermi-liquid critical point. A signature for the unphysical nature of the non-Fermi-liquid critical point associated with the level crossing can be seen by comparing the transverse and longitudinal spin–spin correlation functions. It can be shown that the longitudinal spin–spin correlation function has a non-Fermi-liquid form, but the transverse spin–spin correlation function retains the Fermi-liquid form. As a matter of fact, the level crossing would have occurred had we started from an unphysical model with J_z antiferromagnetic but $J_\perp$ ferromagnetic.

Within the bosonization approach, the meaning of the atomic configurations in the canonically transformed bases is somewhat obscure. The physical content of these configurations becomes transparent once we compare them with the atomic configurations that appear in a perturbation expansion of the original Hamiltonian in terms of $J_\perp/J_z$, $J_\perp/V$, t/J_z, t/V, W/J_z, and W/V. This atomic analysis is carried out in reference [48], from which it is physically clear that the ground state is always a singlet no matter what the value of E_d^0 is. No level crossing is expected!

3.2. Strong-coupling Toulouse point II

This corresponds to $\epsilon_t = 1/2$ and $\epsilon_j = 0$. The Coulomb-gas analysis would again predict this point to be deep in the domain of attraction of the strong-coupling Fermi-liquid phase. The effective Hamiltonian is

$$H_{eff}^B = H_0 + E_d^0 \sum_\sigma \tilde{f}_\sigma^\dagger \tilde{f}_\sigma + t\left[\left(\sum_\sigma \tilde{f}_\sigma^\dagger\right)\eta + \text{HC}\right] - \frac{J_\perp}{4\pi a}(\tilde{f}_\uparrow^\dagger \tilde{f}_\downarrow + \text{HC}) + \left(\frac{\kappa_s}{2\pi\rho_0}\right)\left(\sum_\sigma \sigma\, \tilde{f}_\sigma^\dagger \tilde{f}_\sigma\right)\left(\frac{1}{2\pi}\right)\left(\frac{\mathrm{d}\Phi_s}{\mathrm{d}x}\right)_{x=0}. \tag{20}$$

Here, $\eta_k^\dagger$ denotes a spinless conduction electron band; it comes from refermionizing the charge boson. $\tilde{f}_\sigma^\dagger = X_{\sigma 0} F_\sigma F_\eta^\dagger$ is a pseudofermion operator. Unlike for H_{eff}^A, we have kept only the κ_s-term in ΔH, as the κ_c-term is not important. All of the correlation functions can once again be explicitly determined:

$$\begin{aligned} G_d(\tau) &\sim \frac{\rho_0}{\tau} \\ \chi_\sigma^{-+}(\tau) &\sim \left(\frac{\rho_0}{\tau}\right)^2 \\ \chi_\sigma^{zz}(\tau) &\sim \left(\frac{\kappa_s}{2\pi\rho_0 h_s}\right)^2 \left(\frac{\rho_0}{\tau}\right)^2 \\ \chi_\rho(\tau) &\sim \left(\frac{\rho_0}{\tau}\right)^2 \end{aligned} \tag{21}$$

where κ_s is again the deviation from the Toulouse point. Once again, the long-time behaviour of the single-particle and two-particle correlation functions establishes the strong-coupling, Fermi-liquid nature of this Toulouse point.

Except for the change of sign in $J_\perp$, the effective Hamiltonian (20) is identical to that of references [52] and [51]. Once again, when the Klein operators are properly incorporated in the bosonization representation of the fermion fields, no level crossing occurs.

3.3. The Toulouse point for the intermediate phase

This last Toulouse point occurs at $\epsilon_t = 1$ and $\epsilon_j = 0$. It is not inconsistent with the Coulomb-gas result that these values of the Coulomb-gas stiffnesses lie close to such a boundary (though it is not possible to determine the precise boundary between the intermediate phase and the strong-coupling phase from the Coulomb-gas analysis).

In order to write down the effective Hamiltonian in a convenient fashion, we need to introduce a new basis set for the three levels, $|A\rangle$, $|B\rangle$, and $|0\rangle$. They are defined as follows:

$$\begin{aligned} |A\rangle &= \frac{1}{\sqrt{2}}\sum_\sigma(-\sigma f_\sigma^\dagger F_{\bar\sigma}^\dagger)|\text{vac}\rangle \\ |B\rangle &= \frac{1}{\sqrt{2}}\sum_\sigma(-f_\sigma^\dagger F_{\bar\sigma}^\dagger)|\text{vac}\rangle \\ |0\rangle &= b_0^\dagger|\text{vac}\rangle \end{aligned} \tag{22}$$

where $f_\sigma^\dagger$ and $b_0^\dagger$ are pseudofermion and pseudoboson operators defined in equation (17). In this new basis, $n_d = \sum_\sigma f_\sigma^\dagger f_\sigma = (X_{AA} + X_{BB} - X_{00})$, $S_d^z = (1/2)\sum_\sigma \sigma f_\sigma^\dagger f_\sigma = (X_{AB}+X_{BA})/2$, and $X_{\uparrow\downarrow}F_\downarrow^\dagger F_\uparrow = -X_{AA}+X_{BB}$. The effective Hamiltonian has the following form:

$$\begin{aligned} H_{eff}^C = \sum_{k\sigma} E_k c_{k\sigma}^\dagger c_{k\sigma} + 2t\sqrt{\pi a}[X_{A0}c_\uparrow c_\downarrow + \text{HC}] + \left(E_d^0 - \frac{J_\perp}{4\pi a}\right)X_{AA} + \left(E_d^0 + \frac{J_\perp}{4\pi a}\right)X_{BB} \\ + \frac{\kappa_c}{2\pi\rho_0}(X_{AA} + X_{BB} - X_{00})(c_\uparrow^\dagger c_\uparrow + c_\downarrow^\dagger c_\downarrow) \\ + \frac{\kappa_s}{2\pi\rho_0}(X_{AB} + X_{BA})(c_\uparrow^\dagger c_\uparrow - c_\downarrow^\dagger c_\downarrow). \end{aligned} \tag{23}$$

In this effective Hamiltonian, the charge sector is described by a genuine *charge Kondo* model. $|A\rangle$ and $|0\rangle$ play the role of $|\uparrow\rangle$ and $|\downarrow\rangle$ of the anisotropic spin Kondo problem and should be thought of as objects carrying charge 2 and charge 0, respectively. The transformed hybridization term is the direct analogue of the spin-flip term in the anisotropic spin Kondo problem. The residual interaction in the charge sector, $\kappa_c/2\pi\rho_0$, is the analogue of the longitudinal exchange interaction in the anisotropic spin Kondo problem, with the density playing the role of the spin in the latter. The essential difference between the charge Kondo problem in this mixed-valence context and the spin Kondo problem lies in the symmetry-breaking field. In the latter, the spin rotational invariance guarantees that no explicit magnetic field term will be generated in the absence of an external magnetic field. In our charge Kondo problem, the p–h symmetry is explicitly broken, and the symmetry-breaking field $h^{\text{charge}} = E_d^0 - J_\perp/4\pi a$ is in general non-zero. For the impurity problem, the condition that the renormalized h^{charge} vanishes can be achieved only through fine tuning the bare d level E_d^0 to a critical value E_d^c.

When $h^{\text{charge}} = 0$ is enforced, a zero-temperature quantum phase transition takes place as κ_c is increased through zero. The transition is characterized by a Kosterlitz–Thouless transition in the charge sector; the spin sector is not critical. The phenomenology of the intermediate phase is recovered on the negative-κ_c side, to which the remainder of this section is devoted. Here, the charge sector is described by the weak-coupling fixed points of

the charge Kondo problem, while the spin excitations are described by the strong-coupling, Fermi-liquid-like fixed point of the Kondo problem. A spin–charge separation takes place.

Within the charge sector, the impurity configuration in the ground state is entirely $|0\rangle$ for $h^{\rm charge} < 0$, and $|A\rangle$ for $h^{\rm charge} > 0$. This is the result of infinite charge susceptibility in the corresponding ferromagnetic charge Kondo problem. Exactly at $h^{\rm charge} = 0$—namely, when E_d^0 is tuned to the critical value $E_d^c = J_\perp/4\pi a$—the impurity degrees of freedom in the ground state involve an equal, incoherent, mixture of $|0\rangle$ and $|A\rangle$. Schematically, the ground-state wavefunction can be written as $\phi = |A\rangle\phi_A + |0\rangle\phi_0$ where ϕ_A and ϕ_0 are the wavefunctions of the conduction electrons such that ϕ is the solution to a ferromagnetic Kondo model with zero magnetic field. With $h^{\rm charge} = 0$, the intermediate mixed-valence dynamics applies at all temperatures. When E_d^0 is moved away from the critical value, a finite crossover temperature $T_{co} \sim |E_d^0 - E_d^c|$ emerges. The intermediate mixed-valence dynamics continues to apply at $T > T_{co}$. At low temperatures ($T < T_{co}$), however, the charge fluctuations become gapped out.

The single-particle, density–density, longitudinal and transverse spin–spin correlation functions are given as follows:

$$\begin{aligned} G_d(\tau) &\sim \left(\frac{\rho_0}{\tau}\right)^{[1/2+(1/2)(1-\sqrt{2}\kappa_c/\pi)^2]} \\ \chi_\rho^c(\tau) &\sim \frac{(\rho_0 t)^2}{(-4\kappa_c)}\left(\frac{\rho_0}{\tau}\right)^{(-4\kappa_c)} \\ \chi_\sigma^{-+}(\tau) &\sim \left(\frac{\rho_0}{\tau}\right)^2 \\ \chi_\sigma^{zz}(\tau) &\sim \left(\frac{\kappa_s}{2\pi\rho_0 h_s}\right)^2\left(\frac{\rho_0}{\tau}\right)^2 \end{aligned} \tag{24}$$

where χ_ρ^c labels the connected part. The exponent for the single-particle Green's function is particularly noteworthy. The $\frac{1}{2}$ part is the contribution of the spin degrees of freedom. It is independent of interactions, and is the same value as we would get for a non-interacting problem! The remaining part, $\frac{1}{2}(1-\sqrt{2}\kappa_c/\pi)^2$, is due to the charge degrees of freedom and is interaction dependent. This is consistent with the physical picture that in the intermediate phase the low-lying spin excitations are quasiparticle-like while charge excitations have the non-Fermi-liquid form.

Other correlation functions in the charge sector also have an algebraic behaviour with interaction-dependent exponents, and a pairing susceptibility:

$$\left\langle T_\tau\left(\sum_\sigma c_\sigma d_{\bar\sigma}\right)(\tau)\left(\sum_\sigma d_{\bar\sigma}^\dagger c_\sigma^\dagger\right)(0)\right\rangle \sim \left(\frac{\rho_0}{\tau}\right)^{(\kappa_c/\sqrt{2}\pi)^2} \tag{25}$$

is enhanced compared to the Fermi-liquid case. This makes it plausible that the ground state in the corresponding lattice model is superconducting. In that case, the intermediate mixed-valence dynamics would describe the physics in the normal state, i.e., at temperatures between the transition temperature and some upper cut-off energy scale.

To summarize, the explicit results for the correlation functions at this Toulouse point highlight all of the features expected of an intermediate phase: spin–charge separation; a quasiparticle residue vanishing in a power-law fashion; Fermi-liquid-like spin-correlation functions; and self-similar local charge correlation functions with interaction-dependent exponents. We note in passing that these characteristics bear a strong similarity to those of the Luttinger liquid in one-dimensional interacting fermion systems [17, 18, 13, 14].

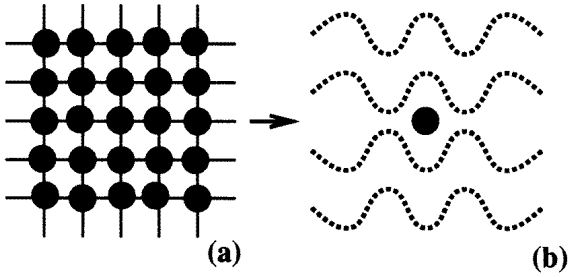

Figure 11. A schematic picture of the lattice model and its reduction to an effective impurity model with a self-consistent conduction electron bath in the large-D limit.

4. The extended Hubbard model as a lattice of Anderson impurities: the large-D limit

We now turn to the lattice model, equation (3), which we suggestively rewrite as

$$H = \sum_i h_i + \sum_{ij} h_{ij}$$

$$h_i = \epsilon_d^0 n_{di} + U n_{di\uparrow} n_{di\downarrow} + t\left(\sum_\sigma d_{i\sigma}^\dagger c_{i\sigma} + \text{HC}\right) + V n_{di} n_{ci} + J \boldsymbol{S}_{di} \cdot \boldsymbol{s}_{ci} \tag{26}$$

$$h_{ij} = t_{ij} \sum_\sigma c_{i\sigma}^\dagger c_{j\sigma}.$$

This is pictorially illustrated in figure 11(a), in which each black dot represents an h_i-term, and across each bond on the lattice there is an h_{ij}-term.

4.1. Mapping to a self-consistent impurity problem in the large-D limit

The limit of infinite dimensions [25, 26] is defined by scaling the hopping term, t_{ij}, in terms of the dimensionality (D) such that the limit is well defined. For the nearest-neighbour hopping

$$t_{\langle ij\rangle} = \frac{t_0}{\sqrt{2D}}. \tag{27}$$

The $D \to \infty$ limit is taken with t_0 kept fixed.

We recall that the large-D limit of a classical non-frustrated lattice spin system is taken by scaling the nearest-neighbour coupling to be of order $1/D$. For any given site, the homogeneous contributions from neighbouring sites add up to an effective field, of order unity, that acts on the spin of the selected site. All other contributions are of finite orders in $1/D$ and vanish in the large-D limit. This is the content of the Weiss molecular-field theory for classical magnets. In the quantum systems, the single-particle hopping contributes to the kinetic energy of the fermion system which, at zero temperature, is the zero-point energy associated with quantum fluctuations. The $1/\sqrt{D}$ scaling in equation (27), as opposed to the $1/D$ scaling, is necessary to capture these quantum fluctuations. With this scaling, the average kinetic energy per unit cell is of order unity in the large-D limit.

In finite dimensions, when on-site interactions are present, a single-particle-hopping term will generate effective inter-site interactions involving two or more particles. With the

single-particle-hopping term being scaled as in equation (27), the interactions generated are of the order of $1/D$ or higher.

For a selected site, say site 0, the effect of the rest of the sites is to generate a retarded Wiess mean field that couples to the single-particle degrees of freedom at site zero. The modifications to the on-site dynamics involving two or more particles are of higher order in $1/D$ and do not survive in the large-D limit. The result is that all local correlation functions of the lattice model can be entirely determined by the following effective on-site action:

$$S_{imp}^{eff} = S_0 - \int_0^\beta \mathrm{d}\tau \int_0^\beta \mathrm{d}\tau' \sum_\sigma c_{0\sigma}^\dagger(\tau) g_0^{-1}(\tau - \tau') c_{0\sigma}(\tau'). \tag{28}$$

S_0 is the action associated with h_0. Since h_0 contains all the local interactions, the procedure treats the local interactions in a dynamical fashion. $g_0^{-1}(\tau - \tau')$, or equivalently its Fourier transform, $g_0^{-1}(\mathrm{i}\omega_n)$, where $\mathrm{i}\omega_n$ is the fermionic Matsubara frequency, is retarded. This is the result of integrating out the degrees of freedom other than those for site 0, at the one-particle level. Pictorially, g_0^{-1} describes the effect of all of the Feynman trajectories in which one electron leaves site zero, explores the lattice, and returns to the origin. Translational invariance demands that the local correlation functions of the lattice model are site independent, and are the same as the correlation functions of the impurity model. This leads to the following self-consistency equation:

$$g_0^{-1}(\mathrm{i}\omega_n) = -\sum_{ij} t_{i0} t_{0j} [G_{ij}(\mathrm{i}\omega_n) - G_{i0}(\mathrm{i}\omega_n) G_{0j}(\mathrm{i}\omega_n)/G_{00}(\mathrm{i}\omega_n)] \tag{29}$$

where $G_{lm}(\tau) \equiv -\langle T_\tau c_{l\sigma}(\tau) c_{m\sigma}^\dagger(0)\rangle_H$ is the lattice Green's function. Equations (28) and (29) define the dynamical mean-field formalism that is exact in the large-D limit [26].

It is physically more transparent to rewrite S^{eff} in the Hamiltonian form. We achieve this by introducing a non-interacting electron bath whose dispersion and coupling to the $c_{0\sigma}$ has to be determined self-consistently. Introducing $\eta_{k\sigma}^\dagger$ and $\eta_{k\sigma}$ as the creation and annihilation operators for this fermion bath, where k is a dummy momentum variable, we can rewrite the effective impurity problem in terms of the following effective impurity Hamiltonian:

$$H_{imp}^{eff} = h_0 + \sum_{k\sigma} t_k (\eta_{k\sigma}^\dagger c_{0\sigma} + \mathrm{HC}) + \sum_{k\sigma} \epsilon_k \eta_{k\sigma}^\dagger \eta_{k\sigma}. \tag{30}$$

The self-consistency equation (29) is equivalent to

$$\sum_k t_k^2/(\mathrm{i}\omega_n - \epsilon_k) = -\sum_{ij} t_{i0} t_{0j} [G_{ij}(\mathrm{i}\omega_n) - G_{i0}(\mathrm{i}\omega_n) G_{0j}(\mathrm{i}\omega_n)/G_{00}(\mathrm{i}\omega_n)]. \tag{31}$$

Pictorially, we have reduced the task of solving the full lattice problem of figure 11(a) into that of solving the problem of a fully interacting quantum impurity embedded in a self-consistent fermionic sea, as is illustrated in figure 11(b).

4.2. Solution to the effective impurity problem

The crucial question is that of the nature of the self-consistent bath. What we found is that, as long as the solution is metallic, the density of states of the fermionic bath at the Fermi energy is *finite*. This is a self-consistent statement. The reasoning goes as follows. Assuming that the bath density of states is finite at Fermi energy, we can proceed to solve the impurity problem in an asymptotically exact fashion by applying the bosonization technique. Among the quantities that can be calculated asymptotically exactly is the local Green's function c_0. That this Green's function has a regular spectral function is seen, in the

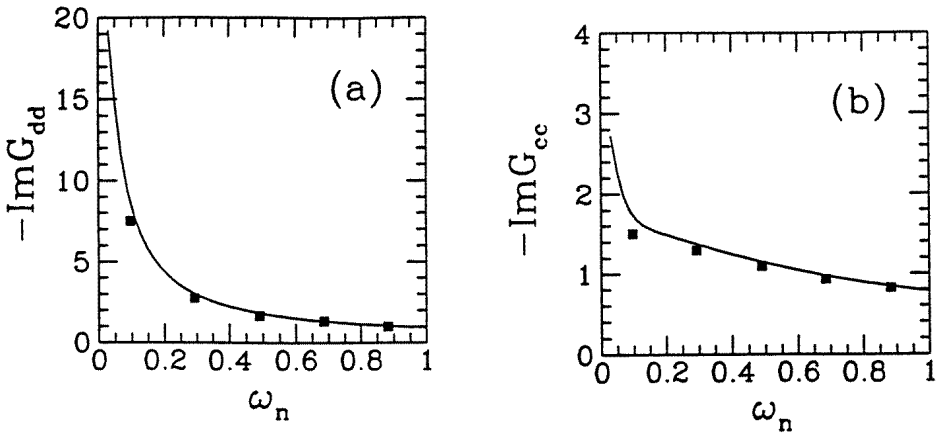

Figure 12. Numerical results of the d- and c-electron Green's functions versus the Matsubara frequency ω_n for a set of parameters for which the solution is a non-Fermi-liquid metallic state. Solid lines come from the self-consistent exact-diagonalization method and the solid squares are from quantum Monte Carlo simulation with $\beta = 64$.

Coulomb-gas representation, by noting that the local c_0 does not create a kink. A regular Green's function c_0 implies a regular self-energy for the c electrons, which, through the self-consistency equation (31), in turn implies that the density of states of the self-consistent fermionic bath is regular! The self-consistency is hence established. This argument applies to any lattice. In the special case of a Lorentzian density of states, this statement is more than asymptotically exact—it is exact. In the case of a Bethe lattice with infinite coordination, we have numerically solved the self-consistency equations [53]. We indeed found that the density of states of the bath fermions at the Fermi energy is finite as long as the solution is metallic. In figure 12, we plot the imaginary part of the d-electron and c-electron Green's functions as functions of the Matsubara frequency. The zero-frequency limit of these Green's functions is identical to the density of states at the Fermi energy. It is clear that, even though the d-electron Green's function is divergent, as expected in the non-Fermi-liquid form discussed in the previous sections, the c-electron density of states is regular.

Armed with this understanding of the fermionic bath, the only essential difference between this self-consistent Anderson model and the single-impurity generalized Anderson model is that this time the effective d level is

$$E_d^{imp} = \epsilon_d^0 - \mu \tag{32}$$

instead of ϵ_d^0. The effective impurity level here is measured with respect to the Fermi energy of the lattice model which is, of course, different for different amounts of electrons.

The fact that the density of states of the self-consistent fermionic bath at the Fermi energy is finite implies that we can carry out an asymptotically exact analysis on the self-consistent generalized Anderson impurity model exactly the way we did for the single-impurity generalized Anderson model. The classification of the possible phases of the single-impurity Anderson model applies to the self-consistent Anderson impurity model, provided that we express the stiffness parameters of the phase diagram, figure 7, in terms of the self-consistent parameters. In particular, there is a metallic non-Fermi-liquid state of the extended Hubbard model that corresponds to the intermediate phase of the impurity model.

As in the impurity model, we have a spin-excitation spectrum that is spin-$\frac{1}{2}$ quasiparticle-like, and a charge-excitation spectrum that is incoherent. What we have is a local route towards spin–charge separation in the extended Hubbard model.

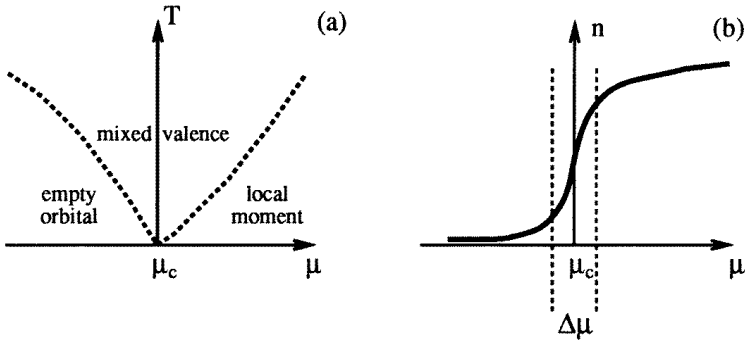

Figure 13. (a) The crossover in terms of the temperature (T) and the chemical potential (μ) for the intermediate phase; (b) the electron density (n) versus the chemical potential for the intermediate phase. $\Delta\mu \sim (T)^{(2\epsilon_t^*-1)}$ where $\epsilon_t^* > 1$ is the renormalized charge-stiffness constant.

The fact that the impurity level of the self-consistent impurity problem is measured with respect to the chemical potential implies that for a model with fixed ϵ_d^0, the temperature–chemical-potential crossover is as given in figure 13(a).

4.3. The pinning of the chemical potential

A remarkable phenomenon takes place. This is the pinning of the chemical potential [85]. The critical chemical potential, at which the mixed-valence state persists to zero temperature, corresponds to a range of electron densities. This can be seen as follows. The local correlation functions of the extended Hubbard model in infinite dimensions are given by the impurity problem. In particular, the occupation numbers of the lattice, for a given chemical potential, can be obtained from the local Green's functions of the corresponding impurity model. It follows from our analysis of the impurity model that, at zero temperature, n_d (and also $n = n_d + n_c$) is a discontinuous function of the chemical potential: $n_d \sim n_d^+ \approx 1 - \mathrm{O}(t^2)$ for $\mu > \mu_c$, while $n_d \sim n_d^- \approx \mathrm{O}(t^2)$ for $\mu < \mu_c$. At finite temperatures, n_d is increased from n_d^- to n_d^+ as μ is increased from $\mu_c - \Delta\mu$ to $\mu_c + \Delta\mu$ where

$$\Delta\mu \sim \Delta_0 (T\xi_0)^{(2\epsilon_t^*-1)}. \tag{33}$$

As long as n_d is inside the range (n_d^-, n_d^+), the condition of equation (12) is satisfied. The correlation functions will be controlled by the intermediate phase at criticality.

It is remarkable that the fact that our impurity model is associated to a lattice problem forces the effective impurity model to be at criticality, with a larger symmetry than we would have naively expected. Physically, for an incoherent state to be metallic, it is necessary to allow charge transfer between the local degrees of freedom and the bath. This can only happen if the local charge degrees of freedom are in equilibrium with the conduction electron bath. This requires the heavy level to be at the chemical potential.

4.4. Further remarks

The RG analysis that leads to the classification of the possible phases of the effective impurity problem discussed in section 2 is based on a small-hybridization expansion. In the context of the low-energy effective Hamiltonians for the high-T_c system, one of the important questions is that of whether the extended Hubbard model can be further reduced to an effective-one-band Hubbard model [86, 87]. One argument used in this context is that, when the hybridization is sufficiently large, it is more appropriate to first diagonalize the problem within a unit cell, leading to the Zhang–Rice singlet [86]. The effective Hamiltonian for the low-energy local orbitals is the so-called t–J Hamiltonian. In the light of this construction, a natural question to ask is that of whether the physics of the extended Hubbard model at large hybridization is different from that at small hybridization. The large-D limit provides a unique opportunity to address this question. This problem has only been numerically studied in the spinless version of the extended Hubbard model [53]. The numerical solution indicates that the qualitative phase diagram is similar for the large- and small-hybridization limits. However, the precise values of the exponents of the correlation functions could be modified as the hybridization is increased. Further work along this direction needs to be carried out.

We have established the existence of metallic non-Fermi-liquid states in the extended-Hubbard-model equation (3) in the large-D limit. What happens in finite dimensions? This is a question which is only beginning to be addressed. Some progress is reported in the next section.

We close this section on a methodological note. Various numerical methods, such as quantum Monte Carlo simulation [88–90] and exact diagonalization [91, 53], can be used to solve the self-consistent dynamical mean-field equations associated with the $D = \infty$ limit. Whatever the means, the solution to these equations should always describe the solution to an impurity coupled to a self-consistent fermionic bath. And it is always instructive to ask (a) what is the nature of the density of states of the self-consistent fermionic bath near its Fermi energy (is it regular, gapped, vanishing with a power law, or singular with a power law, to name a few); and (b) what are the low-lying levels associated with the impurity? Armed with these items of information, it is usually possible to use the RG method or other analytical means to determine the qualitative behaviour of the solution.

5. Competition between the local and short-range fluctuations: the alternative large-D limit

One major advantage of the large-D approach is that of being able to treat local correlations in a fully dynamical fashion. This feature is responsible for the uncovering of the metallic non-Fermi liquids in the extended Hubbard model that other methods have failed to achieve. One major disadvantage of the large-D approach is that spatial fluctuations beyond the one-particle level are all frozen: inter-site interactions reduce to Hartree contributions only. For physical systems in finite dimensions, inter-site RKKY or superexchange-type interactions are expected to compete with local correlations. For instance, an unstable non-Fermi-liquid fixed point arises due to the competition between the inter-impurity RKKY interaction and the local Kondo couplings in the two-impurity Kondo problem [92]. In the Kondo-lattice models, such a competition led to the competition between long-range magnetic ordering and Kondo-singlet formation. In the absence of long-range ordering, the dynamical role of the inter-site interactions in the local Kondo-like physics has largely been left unexplored. From the large-D point of view, one way to recover the spatial fluctuations is via the

perturbative $1/D$ expansion. Truncating the perturbation series to order $(1/D)^n$ requires solving simultaneously clusters containing one, two, ..., $n+1$ sites embedded in their respective self-consistent media [93]. The practicality of this procedure is unclear at this stage. An alternative route is via a loop expansion with the requirement that the $D = \infty$ results be recovered at the saddle-point level, as has been constructed in models with certain forms of quenched disorder [94]. For clean systems, it turns out to be difficult to formulate such a loop expansion.

We have recently introduced an alternative large-D limit to study the interplay between local correlations and short-range spatial fluctuations in the two-band extended Hubbard model [54, 95]. In this procedure, an explicit inter-site density–density interaction term is introduced, and is scaled in terms of the dimensionality such that its *fluctuation part* survives in the large-D limit. This procedure leads to an impurity embedded in a self-consistent fermionic bath *and a self-consistent bosonic bath*. Detailed analysis [54] has so far been carried out only for the spinless version of the extended Hubbard model, given by the following Hamiltonian:

$$H = \sum_i [E_d^0 n_{di} + t(d_i^\dagger c_i + \text{HC}) + V n_{di} n_{ci}] + \sum_{\langle ij \rangle} [t_{ij} c_i^\dagger c_j + v_{ij} {:}n_{di}{::}n_{dj}{:}]. \tag{34}$$

The standard large-D limit is taken with t_{ij} of the form of equation (27) and v_{ij} of order $1/D$. With that scaling, only the static component of v_{ij} gives a non-vanishing contribution in the large-D limit. Hence, inter-site interactions give only a Hartree contribution. The alternative large-D limit is taken with equation (27) and

$$v_{\langle ij \rangle} = v_0/\sqrt{D}. \tag{35}$$

In order to have a well defined large-D limit, it is necessary that the zero-frequency mode, i.e. the Hartree term, be treated separately. In the absence of symmetry breaking, the effect of the Hartree term is a change to the chemical potential. This is handled through normal ordering, ${:}n{:} \equiv n - \langle n \rangle$.

The procedure outlined in the previous section leads to the following effective impurity action:

$$S_{imp}^{eff} = S_0 - \sum_{\mathrm{i}\omega_n} c_0^\dagger(\mathrm{i}\omega_n) g_0^{-1}(\mathrm{i}\omega_n) c_0(\mathrm{i}\omega_n) - \sum_{\mathrm{i}\nu_n \neq 0} n_{d0}(\mathrm{i}\nu_n) \chi_0^{-1}(\mathrm{i}\nu_n) n_{d0}(\mathrm{i}\nu_n). \tag{36}$$

In addition to the self-consistency equation (29), an additional self-consistency equation is required, this one for the density propagator:

$$\chi_0^{-1}(\mathrm{i}\nu_n) = \sum_{ij} v_{i0} v_{0j} [\chi_{ij}(\mathrm{i}\nu_n) - \chi_{i0}(\mathrm{i}\nu_n)\chi_{0j}(\mathrm{i}\nu_n)/\chi_{00}(\mathrm{i}\nu_n)] \tag{37}$$

where $\chi_{lm}(\mathrm{i}\nu_n)$ is the Fourier transform of the lattice density–density correlation function, $\chi_{lm}(\tau) \equiv \langle T_\tau {:}n_l{:}(\tau){:}n_m{:}(0)\rangle_H$. $\mathrm{i}\nu_n$ is the bosonic Matsubara frequency.

The effective action can once again be written in terms of a single-impurity Hamiltonian. In our spinless case, this is a self-consistent resonant-level model with an additional screening bosonic bath:

$$H_{imp}^{eff} = (\epsilon_d^0 - \mu) n_{d0} + t(d_0^\dagger c_0 + \text{HC}) + V n_{d0} n_{c0} + \sum_k t_k(\eta_k^\dagger c_0 + \text{HC}) + \sum_k \epsilon_k \eta_k^\dagger \eta_k + \sum_q F_q(\rho_q + \rho_{-q}^\dagger){:}n_{d0}{:} + \sum_q W_q \rho_q^\dagger \rho_q. \tag{38}$$

Here, $\eta_k^\dagger$ creates, like in the previous section, a fermionic bath with a dummy momentum variable k. The dispersion, ϵ_k, and the hybridization coupling parameter, t_k, are to be

determined self-consistently. Likewise, $\rho_q^\dagger$ creates a bosonic bath with a dummy momentum variable q. The corresponding self-consistent dispersion and coupling parameters are W_q and F_q.

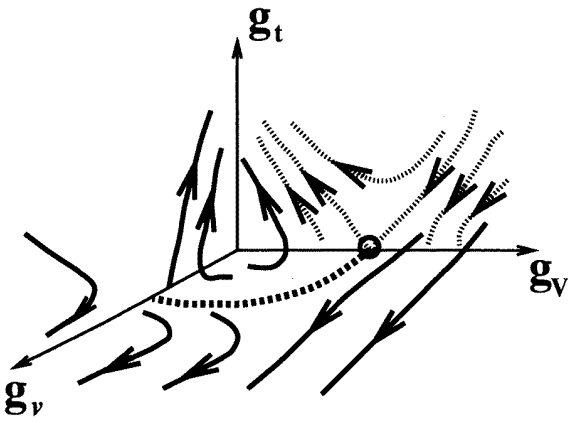

Figure 14. The phase diagram of the Hamiltonian equation (34) in the mixed-valence regime. $g_t = t\rho_0$, $g_V = [1 - (2/\pi)\tan^{-1}(\pi\rho_0 V/2)]$, and $g_v = \rho_0 v_0$. The circle labels a Kosterlitz–Thouless critical point. The dashed line is schematic. The different phases are described in the text.

Detailed analysis shows that, in this case, the fermionic bath density of states remains regular. The spectral function of the bosonic bath, however, can be highly non-ohmic. This is fortunate, for an impurity model with a fermionic bath having an arbitrary form of density of states near the Fermi energy is quite difficult to handle [96–98]. On the other hand, an impurity model coupled to a bosonic bath with non-ohmic spectral function can still be analysed asymptotically exactly, within a modified kink-gas picture. Details are given in reference [54]. The most interesting regime is again the mixed-valence regime, for which the renormalized effective impurity level is zero. The self-consistent solution is shown in figure 14. The phase diagram is specified in terms of three parameters, $g_t = \rho_0 t$, $g_V = [1 - (2/\pi)\tan^{-1}(\pi\rho_0 V/2)]$, and $g_v = \rho_0 v_0$. They are essentially the dimensionless hybridization, on-site density–density interactions, and inter-site density–density interactions.

At $g_v = 0$, the problem reduces to the usual large-D case discussed in the previous section [53]. For our spinless problem, a Kosterlitz–Thouless transition takes place describing the charge Kondo effect [74]. When $g_V < g_V^{crit}$, i.e., $-V < V_0^{crit}$, the solution is a Fermi liquid. For $g_V > g_V^{crit}$, i.e., $-V > V_0^{crit}$, the solution is a line of non-Fermi liquids with the connected local density susceptibility:

$$\chi(\tau) \approx (\rho_c/\tau)^\alpha. \tag{39}$$

The exponent α is interaction dependent, increasing from 0 to 2 as one moves away from the critical point [99, 100].

The inter-site interaction v_0 modifies the phase diagram in several ways. Consider first $g_V > g_V^{crit}$. The line of fixed points of the $v_0 = 0$ problem becomes unstable. Remarkably, the correlation functions in the new fixed points can be determined. In fact, they have the same form as is given in equation (39).

For $g_V < g_V^{crit}$, we are able to establish the existence of a phase transition as v_0 is increased. For sufficiently strong v_0, the solution must be a non-Fermi liquid. Physically,

the inter-site density–density interactions provide charge screening, which contributes to the orthogonality effect. In the mixed-valence regime, this orthogonality helps realize the weak-coupling fixed point with incoherent charge excitations. For sufficiently small v_0, on the other hand, the Fermi-liquid solution is stable.

As a result, non-Fermi liquids with self-similar correlation functions occur even for repulsive values of the on-site density–density interaction. It is therefore not necessary to require attractive on-site interactions to realize the incoherent charge state.

A finite inter-site interaction v_0 also changes the nature of the phase transition. We have shown that [54] the phase transition is not of the Kosterlitz–Thouless type. We have been unable to establish the precise nature of the phase transition.

The self-consistent equations and the kink-gas analysis can also be carried out in the spinful extended Hubbard model. The form of scaling equations implies that the results derived here for the spinless model carries over to the charge sector of the spin–charge-separated intermediate phase [101].

The formalism outlined in this section can be generalized to various different contexts. The effects of inter-site spin-exchange interactions are the obvious next problem to study. Inter-site interactions of three or more particles can also be treated along this line.

6. Conclusions, new insights, and open questions

The focus of this article has been on the competition between local charge and local spin fluctuations, both in the single-impurity Anderson model and in the lattice extended Hubbard model. We have found that such a competition leads to metallic non-Fermi liquids in certain interaction parameter ranges. In particular, we have identified a novel non-Fermi-liquid mixed-valence state, called the intermediate phase. This phase displays the phenomenon of spin–charge separation. The low-energy spin excitations are much like that of the strong-coupling Fermi-liquid phase that one would derive from, for instance, the slave-boson condensed phase within the slave boson large-N approach. The charge excitations are distinctively of a non-Fermi-liquid form.

Are these non-Fermi-liquid states relevant to real materials? For single-impurity problems, these non-Fermi-liquid phases can be realized only when the impurity level is tuned to be close to the Fermi energy of the conduction electrons. We can envisage two contexts in which this kind of fine tuning of the impurity level is physically feasible. The first is in the context of dilute impurities in metals. The Fermi level of the conduction electron sea can be varied by substituting for some of the elements in the compound with ones of different valency. Called Fermi-level tuning, this mechanism has already been invoked to explain the trend of the Kondo energy in certain uranium-based heavy fermions [102, 103]. Valence fluctuations in uranium-based compounds are in general much stronger than those in cerium-based compounds. It is conceivable that some of them have interaction parameters that fall in the domain of the intermediate phase. Systematic studies of the Fermi-level-tuning phenomenon, therefore, can play a significant role in the current search for and study of non-Fermi liquids in f-electron-based materials. The second context where impurity levels can be tuned is in mesoscopic systems. This time, the tuning is achieved through biasing the confined area with respect to the leads [104]. In both cases, the accuracy required for tuning the Fermi level is Δ^*/w, where Δ^* is the renormalized resonance width, and w is the conduction electron bandwidth.

For lattice problems, the level-tuning requirement is much less stringent. This is the result of the phenomenon of the pinning of the chemical potential, discussed extensively in section 4. There is a range of electron density over which the *effective* impurity level lies

close to the Fermi level of the self-consistent fermion bath. Our findings of the existence of both the strong-coupling and intermediate phases in the mixed-valence regime provide new insights into the similarities of and differences between the heavy fermions and high-T_c cuprates, mentioned at the beginning of this article. The spin dynamics of the intermediate phase and the strong-coupling phase are similar, both displaying a crossover from the high-temperature local moment regime into the low-temperature coherent regime. The charge dynamics, on the other hand, is qualitatively different in these two phases. In the strong-coupling Fermi-liquid phase, the charge dynamics tracks with the spin dynamics. In the intermediate phase, the charge dynamics has non-Fermi-liquid behaviour characterized by the correlation functions discussed in sections 2 and 3.

The phenomenology of the conventional heavy fermions, such as $CeCu_6$ and UPt_3, is well described by the strong-coupling Fermi-liquid phase. Can the normal state of the high-T_c cuprates be described by the intermediate phase? The contrasting behaviours seen in the temperature dependences of the NMR relaxation rate and the electrical resistivity of the cuprates (figure 2), when viewed in the context of those of the heavy fermions (figure 1), are consistent with the qualitative differences between the spin dynamics and charge dynamics expected in the intermediate phase. However, these two quantities measure very different correlation functions. The NMR relaxation rate measures mainly the momentum-($\boldsymbol{q}$-) averaged spin response, while the electrical resistivity measures the $\boldsymbol{q} = 0$ electrical current–current correlation function. Therefore, the precise implications of the contrasting temperature dependences of these two quantities in the cuprates are hard to specify. One clear-cut probe of the relationship between the spin and charge excitations would be that of comparing the temperature dependences of the electron spin resistivity and the electrical resistivity [105]. This requires experimental measurement of the electron spin-diffusion constant.

Our results also raise a number of theoretical questions. Unlike for the multi-channel Kondo problem, the lattice model that we have studied, equation (3), has a well defined limit of vanishing interactions, $U \to 0$, $V \to 0$ and $J \to 0$. In this limit of vanishing interactions, and for dimensions higher than one, the perturbative RG analysis [19] would identify no instability towards a metallic non-Fermi-liquid state. By focusing on the strong-coupling limit, $U = \infty$, and taking the limit of infinite dimensions, $D = \infty$, we have identified non-Fermi-liquid solutions. Obvious questions arise. (a) What happens as the on-site Hubbard interaction U gradually decreases from infinity, all the way to $U = 0$? If a phase transition takes place, is it also of the Kosterlitz–Thouless form? (b) What happens when the dimensionality D decreases from infinity to physical dimensions? The approach outlined in section 5 provides a starting point for addressing one aspect of the finite-dimensionality effects, namely the competition between the on-site and inter-site correlations. The results summarized there imply that the non-Fermi-liquid phases survive the short-range spatial fluctuations. The critical behaviour of the quantum phase transition from the Fermi-liquid to non-Fermi-liquid states, on the other hand, is strongly modified by the spatial correlations. As for (a), it remains an open problem at the present time.

Acknowledgments

I am most grateful to G Kotliar, M Rozenberg, A E Ruckenstein, and J L Smith for stimulating collaborations on this work, and to E Abrahams, J Cardy, V Dobrosavljević, A M Finkelstein, E Fradkin, A Georges, T Giamarchi, K Ingersent, A J Leggett, I Perakis, A J Schofield, A Sengupta, C Sire, C M Varma, Yu Lu, and X Y Zhang for useful discussions and/or communications. I would like to acknowledge the hospitality of the Institute for

Theoretical Physics, University of California at Santa Barbara, and of the Aspen Center for Physics. This research was supported in part by NSF Grant No PHY94-07194 and by an A P Sloan Fellowship.

References

[1] Landau L D 1956 *Sov. Phys.–JETP* **3** 920; 1957 *Sov. Phys.–JETP* **5** 101; 1959 *Sov. Phys.–JETP* **8** 70
[2] Wheatley J 1975 *Rev. Mod. Phys.* **47** 415
[3] Leggett A J 1975 *Rev. Mod. Phys.* **47** 331
[4] McWhan D B and Rice T M 1969 *Phys. Rev. Lett.* **22** 887
[5] Brinkman W F and Rice T M 1970 *Phys. Rev.* B **2** 4302
[6] Mott N F 1990 *Metal–Insulator Transitions* (London: Taylor & Francis)
[7] Grewe N and Steglich F 1991 *Handbook on the Physics and Chemistry of Rare Earths* vol 14, ed K A Gschneidner Jr and L Eyring (Amsterdam: Elsevier) p 343
[8] Lee P A, Rice T M, Serene J W, Sham L J and Wilkins J W 1986 *Comment. Condens. Matter Phys.* **12** 99
[9] For the latest developments, see
Batlogg B, Chu W K and Gubser D (ed) 1996 *Proc. 10th Anniversary HTS Workshop on Physics, Materials and Applications (Houston, TX, 1996)* (Singapore: World Scientific)
[10] Maple M B, Seaman C L, Gajewski D A, Dalichaouch Y, Barbetta V B, de Andrade M C, Mook H A, Lukefahr H G, Bernal O O and MacLaughlin D E 1994 *J. Low Temp. Phys.* **95** 225
[11] Pfleiderer C, McMullan G J and Lonzarich G G 1995 *Physica* B **206+207** 847
Grosche F M, Pfleiderer C, McMullan G J, Lonzarich G G and Bernhoeft N R 1995 *Physica* B **206+207** 20
Julian S R, Mathur N D, Grosche F M and Lonzarich G G 1996 *Preprint*
[12] von Löhneysen H, Pietrus T, Portisch G, Schlager H G, Schröder A, Sieck M and Trappmann T 1994 *Phys. Rev. Lett.* **72** 3262
Bogenberger B and von Löhneysen H 1995 *Phys. Rev. Lett.* **74** 1016
[13] Jerome D and Schulz H J 1982 *Adv. Phys.* **31** 299
Bourbonnais C 1995 *Strongly Interacting Fermions and High T_c Superconductivity* ed B Doucot and J Zinn-Justin (Amsterdam: Elsevier–North-Holland)
[14] Voit J 1995 *Rep. Prog. Phys.* **58** 977
[15] Ralph D C, Ludwig A W W, von Delft J and Buhrman R A 1994 *Phys. Rev. Lett.* **72** 1064; 1995 *Phys. Rev. Lett.* **75** 770
[16] Wingreen N S, Altshuler B L and Meir Y 1995 *Phys. Rev. Lett.* **75** 769
[17] Emery V J 1979 *Highly Conducting One-dimensional Solids* ed J T Devreese *et al* (New York: Plenum)
Solyom J 1979 *Adv. Phys.* **28** 201
[18] Haldane F D M 1981 *J. Phys. C: Solid State Phys.* **14** 2585
[19] Shankar R 1994 *Rev. Mod. Phys.* **66** 129
[20] Castellani C, Di Castro C and Metzner W 1994 *Phys. Rev. Lett.* **72** 316
[21] Engelbrecht J R and Randeria M 1990 *Phys. Rev. Lett.* **65** 1032; 1992 *Phys. Rev.* B **45** 12 419
[22] Anderson P W 1990 *Phys. Rev. Lett.* **64** 1839; 1990 *Phys. Rev. Lett.* **65** 2306
[23] Hewson A C 1993 *The Kondo Problem to Heavy Fermions* (Cambridge: Cambridge University Press)
[24] Nozières P and Blandin A 1980 *J. Physique* **41** 193
[25] Metzner W and Vollhardt D 1989 *Phys. Rev. Lett.* **62** 324
[26] For a comprehensive and updated review, see
Georges A, Kotliar G, Krauth W and Rozenberg M J 1996 *Rev. Mod. Phys.* **68** 13
Earlier reviews on this subject include
Muller-Hartmann E 1989 *Int. J. Mod. Phys.* **3** 2169
Vollhardt D 1991 *Physica* B **169** 277
Georges A, Kotliar G and Si Q 1992 *Int. J. Mod. Phys.* B **6** 705
Pruschke T, Jarrell M and Freericks J K 1995 *Adv. Phys.* **44** 187
[27] Cox D 1987 *Phys. Rev. Lett.* **59** 1240
Jarrell M, Pang H, Cox D L and Luk K H 1996 *Phys. Rev. Lett.* **77** 1612
[28] Asayama K, Kitaoka Y and Kohori Y 1988 *J. Magn. Magn. Mater.* **76+77** 449
[29] Penney T, Milliken F P, von Molnar S, Holtzberg F and Fisk Z 1986 *Phys. Rev.* B **34** 5959
[30] Presumably the dominant contribution to $(1/T_1)_{Cu}$ comes from the f-electron spin fluctuations; there is no symmetry reason for the latter to be filtered out due to special form factors of the hyperfine coupling.

[31] Anderson P W, Yuval G and Hamann D R 1970 *Phys. Rev.* B **1** 4464
[32] Wilson K G 1975 *Rev. Mod. Phys.* **47** 773
[33] Andrei N, Furuya K and Lowenstein J H 1983 *Rev. Mod. Phys.* **55** 331
Tsvelik A M and Wiegmann P B 1983 *Adv. Phys.* **32** 453
[34] Miranda E, Dobrosavljević V and Kotliar G 1996 *J. Phys.: Condens. Matter* **8** 9871
[35] Aronson M C, Osborn R, Robinson R A, Lynn J W, Chau R, Seaman C L and Maple M B 1995 *Phys. Rev. Lett.* **75** 725
Aronson M C, Maple M B, de Sa P, Tsvelik A M and Osborn R 1996 *Preprint*
[36] Imai T, Slichter C P, Yoshimura K and Kosuge K 1993 *Phys. Rev. Lett.* **70** 1002
[37] Takagi H, Batlogg B, Kao H L, Kwo J, Cava R J, Krajewski J J and Peck W F Jr 1992 *Phys. Rev. Lett.* **69** 2975
[38] Hayden S M, Aeppli G, Mook H A, Perring T G, Mason T E, Cheong S-W and Fisk Z 1996 *Phys. Rev. Lett.* **76** 1344
Si Q, Zha Y and Levin K 1994 *J. Appl. Phys.* **76** 6935
[39] Si Q, Kim J H, Lu J P and Levin K 1990 *Phys. Rev.* B **42** 1033
[40] Bonn D A, Liang R, Riseman T M, Baar D J, Morgan D C, Zhang K, Dosanjh P, Duty T L, MacFarlane A, Morris G M, Brewer J H, Kallin C and Berlinsky A J 1993 *Phys. Rev.* B **47** 11 314
[41] Krishana K, Harris J M and Ong N P 1995 *Phys. Rev. Lett.* **75** 3529
[42] Emery V 1987 *Phys. Rev. Lett.* **58** 2794
[43] Varma C M, Schmitt-Rink S and Abrahams E 1987 *Solid State Commun.* **62** 681
[44] This model is not to be confused with the one-band extended Hubbard model. The latter refers to the standard Hubbard model generalized to include nearest-neighbour or further-neighbour interactions.
[45] Si Q and Kotliar G 1993 *Phys. Rev. Lett.* **70** 3143
[46] Si Q and Kotliar G 1993 *Phys. Rev.* B **48** 13 881
[47] Kotliar G and Si Q 1993 *Phys. Scr.* T **49** 165
[48] Kotliar G and Si Q 1996 *Phys. Rev.* B **53** 12 373
[49] Perakis I, Varma C M and Ruckenstein A E 1993 *Phys. Rev. Lett.* **70** 3467
[50] Giamarchi T, Varma C M, Ruckenstein A E and Nozières P 1993 *Phys. Rev. Lett.* **70** 3967
[51] Zhang G M and Yu Lu 1994 *Phys. Rev. Lett.* **72** 2474
Zhang G M, Su Z B and Yu Lu 1996 *Phys. Rev.* B **53** 715
[52] Sire C, Varma C M, Ruckenstein A E and Giamarchi T 1994 *Phys. Rev. Lett.* **72** 2478
[53] Si Q, Rozenberg M, Kotliar G and Ruckenstein A E 1994 *Phys. Rev. Lett.* **72** 2761
[54] Si Q and Smith J L 1996 *Phys. Rev. Lett.* **77** 3391
[55] Coleman P 1984 *Phys. Rev.* B **29** 3035
[56] Read N and Newns D M 1983 *J. Phys. C: Solid State Phys.* **16** 3273
[57] Auerbach A and Levin K 1986 *Phys. Rev. Lett.* **57** 877
[58] Millis A J and Lee P A 1987 *Phys. Rev.* B **35** 3394
[59] Falicov L M and Kimball J C 1969 *Phys. Rev. Lett.* **22** 997
[60] Schrieffer J R and Wolff P A 1966 *Phys. Rev.* **149** 491
[61] Affleck I and Ludwig A W W 1991 *Nucl. Phys.* B **360** 641
[62] Varma C M and Yafet Y 1976 *Phys. Rev.* B **13** 2950
Varma C M 1976 *Rev. Mod. Phys.* **48** 219
[63] Haldane F D M 1978 *Phys. Rev. Lett.* **40** 416; 1978 *J. Phys. C: Solid State Phys.* **11** 5015
[64] Krishnamurthy H R, Wilson K G and Wilkins J W 1980 *Phys. Rev.* B **21** 1044
[65] For recent theoretical discussions see, for example,
Furukawa N 1994 *J. Phys. Soc. Japan* **63** 3214
Millis A J, Littlewood P B and Shraiman B I 1995 *Phys. Rev. Lett.* **74** 5144
Roder H, Zang J and Bishop A R 1996 *Phys. Rev. Lett.* **76** 1356
Sarkar S 1996 *J. Phys.: Condens. Matter* **8** L515
[66] Haldane F D M 1977 *Phys. Rev.* B **15** 2477
[67] Guinea F, Hakim V and Muramatsu A 1985 *Phys. Rev.* B **32** 4410
[68] Aeppli G and Fisk Z 1992 *Comment. Condens. Matter Phys.* **16** 155
[69] Rice T M and Ueda K 1985 *Phys. Rev. Lett.* **55** 995
[70] Brandow B H 1988 *Phys. Rev.* B **37** 250
[71] Grilli M, Raimondi R, Castellani C, Di Castro C and Kotliar G 1990 *Phys. Rev. Lett.* **66** 1236
[72] Cardy J L 1981 *J. Phys. A: Math. Gen.* **14** 1407
See also
Chakravarty S and Hirsch J 1982 *Phys. Rev.* B **25** 3273

[73] Leggett A J, Chakravarty S, Dorsey A T, Fisher M P A and Zwerger W 1987 *Rev. Mod. Phys.* **59** 1 (erratum: 1995 **67** 215)
[74] Wiegmann P B and Finkelstein A M 1978 *Sov. Phys.–JETP* **48** 102
[75] Schlottmann P 1982 *Phys. Rev.* B **25** 4815
[76] Kane C L and Fisher M P A 1992 *Phys. Rev.* B **46** 15 233
[77] For a review, see
Sachdev S 1995 *Proc. 19th IUPAP Int. Conf. on Statistical Physics (Xiamen, People's Republic of China)* ed B-L Hao (Singapore: World Scientific) at press
[78] Furusaki A and Nagaosa N 1993 *Phys. Rev.* B **47** 4631
[79] Nozières P 1974 *J. Low Temp. Phys.* **17** 31
[80] While the Kondo problem and the usual Anderson model with infinite bandwidth are exactly soluble using the Bethe *ansatz* method [33] and conformal field theory [61], the Anderson model with an additional density–density interaction has not been solved this way.
[81] Toulouse G 1969 *C. R. Acad. Sci., Paris* **268** 1200
[82] Heidenreich R, Seiler R and Uhlenbrock D A 1980 *J. Stat. Phys.* **22** 27 and references therein
[83] Neuberger H 1975 *Thesis* Tel Aviv University
[84] Blume M, Emery V J and Luther A 1971 *Phys. Rev. Lett.* **26** 1547
Emery V J and Luther A 1974 *Phys. Rev.* B **9** 215
[85] Si Q, Kotliar G and Georges A 1992 *Phys. Rev.* B **46** 1261
[86] Zhang F C and Rice T M 1988 *Phys. Rev.* B **37** 3759
[87] Emery V J and Reiter G 1990 *Phys. Rev.* B **41** 7247
[88] Jarrell M 1992 *Phys. Rev. Lett.* **69** 168
[89] Rozenberg M, Zhang X Y and Kotliar G 1992 *Phys. Rev. Lett.* **69** 1236
[90] Georges A and Krauth W 1992 *Phys. Rev. Lett.* **69** 1240
[91] Caffarel M and Krauth W 1994 *Phys. Rev. Lett.* **72** 1545
[92] Jones B A, Varma C M and Wilkins J W 1988 *Phys. Rev. Lett.* **61** 125
[93] Schiller A and Ingersent K 1995 *Phys. Rev. Lett.* **75** 113
[94] Dobrosavljević V and Kotliar G 1994 *Phys. Rev.* B **50** 1430
[95] Kajueter and Kotliar have independently constructed related mean-field equations in the context of a spinless one-band fermion model with a semi-circular density of states:
Kotliar G 1996 private communications
Kajueter H 1996 *PhD Thesis* Rutgers University, Piscataway, NJ
[96] Withoff D and Fradkin E 1990 *Phys. Rev. Lett.* **64** 1835
Cassanello C R and Fradkin E 1996 *Phys. Rev.* B **53** 15 079
[97] Ingersent K 1996 *Phys. Rev.* B at press
[98] Si Q 1996 unpublished
[99] Bhattacharjee J, Chakravarty S, Richardson J L and Scalapino D J 1981 *Phys. Rev.* B **24** 3862
[100] Imbrie J Z and Newman C M 1988 *Commun. Math. Phys.* **118** 303
[101] Smith J L and Si Q 1996 unpublished
[102] Kang J S, Allen J W, Maple M B, Torikachvili M S, Ellis W P, Pate B B, Shen Z X, Yeh J J and Linday I 1989 *Phys. Rev.* B **39** 13 529
[103] Maple M B, Gajewski D A, Seaman C L and Allen J W 1994 *Physica* B **199+200** 423
[104] See, for example,
Kastner M 1993 *Phys. Today* **46** 24
[105] Si Q 1996 *Preprint* cond-mat/9507050; 1996 *Proc. 10th Anniversary HTS Workshop on Physics, Materials and Applications (Houston, TX, 1996)* ed B Batlogg, W K Chu and D Gubser (Singapore: World Scientific)
[106] Costi T A 1996 *Preprint*